2016

Lattice QCD Calculation of the Momentum Fraction Carried by Quarks in the Nucleon, and the Roper Puzzle

Mingyang Sun
University of Kentucky, mingyang.sun@uky.edu
Digital Object Identifier: https://doi.org/10.13023/ETD.2016.504

STUDENT AGREEMENT:

I represent that my thesis or dissertation and abstract are my original work. Proper attribution has been given to all outside sources. I understand that I am solely responsible for obtaining any needed copyright permissions. I have obtained needed written permission statement(s) from the owner(s) of each third-party copyrighted matter to be included in my work, allowing electronic distribution (if such use is not permitted by the fair use doctrine) which will be submitted to UKnowledge as Additional File.

I hereby grant to The University of Kentucky and its agents the irrevocable, non-exclusive, and royalty-free license to archive and make accessible my work in whole or in part in all forms of media, now or hereafter known. I agree that the document mentioned above may be made available immediately for worldwide access unless an embargo applies.

I retain all other ownership rights to the copyright of my work. I also retain the right to use in future works (such as articles or books) all or part of my work. I understand that I am free to register the copyright to my work.

REVIEW, APPROVAL AND ACCEPTANCE

The document mentioned above has been reviewed and accepted by the student's advisor, on behalf of the advisory committee, and by the Director of Graduate Studies (DGS), on behalf of the program; we verify that this is the final, approved version of the student's thesis including all changes required by the advisory committee. The undersigned agree to abide by the statements above.

Mingyang Sun, Student

Dr. Keh-Fei Liu, Major Professor

Dr. Christopher Crawford, Director of Graduate Studies

LATTICE QCD CALCULATION OF MOMENTUM FRACTION CARRIED BY QUARKS IN THE NUCLEON, AND THE ROPER PUZZLE

DISSERTATION

A dissertation submitted in partial fulfillment of the
requirements for the degree of Doctor of Philosophy in the
College of Art and Science at the University of Kentucky

By

Mingyang Sun

Lexington, Kentucky

Director: Prof. K.-F. Liu, Professor of the Department of Physics and Astronomy

Lexington, Kentucky

ABSTRACT OF DISSERTATION

LATTICE QCD CALCULATION OF MOMENTUM FRACTION CARRIED BY QUARKS IN THE NUCLEON, AND THE ROPER PUZZLE

This thesis is concerned with the lattice QCD calculation of the momentum fraction carried by quarks in the nucleon. Particularly, the strange quark contribution, $\langle x \rangle_s$, is calculated, as well as the ratio of the strange $\langle x \rangle$ to that of u/d in the disconnected insertion which will be useful in constraining the global fit of parton distribution functions at small x. The disconnected insertion is known to be hard to calculate on the lattice. We adopt the overlap fermion action on several $2+1$ flavor domain-wall fermion ensembles with a light sea quark mass which corresponds to pion mass of 330 MeV and 139 MeV. Smeared grid sources with Z_3 noise are deployed to calculate the nucleon propagator with low-mode substitution. Even-odd grid sources and the time-dilution technique with stochastic noises are used to calculate the high mode contribution to the quark loop. Low mode averaging (LMA) for the quark loop is applied to reduce the statistical error of the disconnected insertion calculation. We also address the puzzle on the mass of the Roper resonance. Using overlap fermion on top of domain-wall fermion configurations, as well as using the clover fermion action, we explore various smeared sources, and use the variational approach to isolate the Roper. We explain why chiral symmetry is important in resolving the discrepancies between lattice calculations and experiment.

KEYWORDS: Lattice QCD, Hadron Structure, Roper, Chiral Symmetry

Mingyang Sun

12/5/2016

LATTICE QCD CALCULATION OF MOMENTUM FRACTION CARRIED BY QUARKS IN THE NUCLEON, AND THE ROPER PUZZLE

By

Mingyang Sun

Keh-Fei Liu

Director of Dissertation

Christopher Crawford

Director of Graduate Studies

12/5/2016

Table of Contents

TABLE OF CONTENTS

List of Tables

List of Figures

Chapter 1

Introduction

Quantum chromodynamics (QCD) is the fundamental quantum field theory of quarks and gluons, which we believe are the basic degrees of freedom that make up hadronic matter. Unlike QED which describes electrons and photons, QCD has the profound property of asymptotic freedom and confinement. At large energy scale, coupling constant is small, and perturbation theory has been applied with great success. On the other hand, at the scale of the hadronic world, the coupling constant is of order unity and perturbative methods fail. In this domain, lattice QCD provides a non-perturbative framework for calculating the hadronic spectrum and matrix element of any operator within these hadronic states from first principles.

Lattice QCD is formulated on a discretized Euclidean space time grid. The grid serves two purposes. First, it is a non-perturbative way to regularize the theory. The finite lattice spacing a provides an ultraviolet cutoff at π/a, and there is no infinity in the system. Continuum limit $a \to 0$ can be taken on physical quantities after the calculation, and thus remove lattice artifacts in the result. Second, discretization is a mean to simulate QCD on a computer using methods that are analogous to that for statistical mechanics systems. With this approach, statistical errors are controlled. One may seek arbitrarily small statistical error given enough computation power. With the recent advancements in computer technology, lattice QCD results are comparable or better to those from experiments in terms of accuracy, and can serve as inputs to phenomenological studies.

Another very useful feature of lattice QCD is that it allows tuning of parameters. It is a common practice to vary quark masses in a wide region in order to study its effect on various hadronic quantities. One may also seek to vary the number of flavors in lattice QCD, to probe into the so-called "large-N" physics. Fermions can also be completely removed in order to study the properties of a pure gauge theory.

Despite the many applications of lattice QCD, this thesis will focus on introducing lattice QCD itself, as well as its application in two topics in hadronic physics.

The first is to calculate the disconnected contribution to the momentum fraction carried by quarks in the nucleon. Ever since the EMC experiment showed that the proton spin carried by quarks is small [1], large effort has been made in both the experimental and the theoretical frontiers to identify all the contributions to the nucleon spin. Calculating the momentum fraction $\langle x \rangle$ is an integral part of the study of this subject. Experimentally, this quantity is only measured indirectly, and fitted with models. Lattice QCD provides a direct calculation, which can be used as input for global analysis.

Another topic will be covered is the disentanglement of the Roper puzzle. As a rare example of parity reversal, the Roper resonance has been an intriguing subject since its discovery. The $SU(6)$ quark model and the relativistic quark model fail to predict the mass of Roper resonance correctly. Since the quenched era, extensive effort has been taken to calculate the Roper mass in first principle by the lattice community; however results from all calculations except the ones with overlap fermion appear to be high. This indicates the dynamical nature of Roper, and its sensitivity to chiral symmetry. In this thesis, we explain the discrepancy on the Roper mass in the lattice community, and calculate the Roper mass.

Chapter 2

QCD on the Lattice

2.1 Putting QCD on the lattice

In order to calculate QCD on the lattice, one has to Wick rotate the spacetime to the Euclidean space first. Suppose x and p are the spatial and momentum coordinates, and the γ's denotes Dirac Gamma matrices, then

$$x_4^E = ix_0^M, \quad x_i^E = -x_i^M, \tag{2.1}$$

$$p_4^E = -ip_0^M = iE, \quad p_i^E = -p_i^M, \tag{2.2}$$

$$\gamma_4^E = \gamma_0^M, \quad \gamma_i^E = i\gamma_i^M, \quad \gamma_5^E = \gamma_5^M, \quad \gamma_5^E = \gamma_1^E\gamma_2^E\gamma_3^E\gamma_4^E, \tag{2.3}$$

with $i = 1, 2, 3$.

From now on, all quantities are in Euclidean space by default, unless specified otherwise.

Consider the continuum vacuum expectation of an operator O,

$$\langle 0|O|0\rangle = \frac{\int \mathcal{D}\bar{\psi}\mathcal{D}\psi\mathcal{D}A\, O(\psi,\bar{\psi},A)\exp(-S_G(A) - S_F(\psi,\bar{\psi},A))}{\int \mathcal{D}\psi\mathcal{D}\bar{\psi}\mathcal{D}A\, \exp(-S_G(A) - S_F(\psi,\bar{\psi},A))}, \tag{2.4}$$

in which S_G is the gauge action, and S_F is the fermion action. The gauge field $A_\mu = A_\mu^a T_a$, in which T_a are the generators of the $SU(3)$ group. The field strength tensor is defined as

$$F_{\mu\nu}^a = \partial_\mu A_\nu^a - \partial_\nu A_\mu^a + g_0 f_{abc} A_\mu^b A_\nu^c. \tag{2.5}$$

Therefore the pure gauge action is

$$S_G(A) = \frac{1}{2}\,\mathrm{Tr}\int d^4x\, F_{\mu\nu}^a F_{\mu\nu}^a, \tag{2.6}$$

and the fermion action is

$$S_F(\psi,\bar{\psi},A) = \int d^4x\, \bar{\psi}(x)(\gamma_\mu D_\mu + m)\psi(x), \tag{2.7}$$

in which D_μ is the covariant derivative

$$D_\mu = \partial_\mu + ig_0 A_\mu, \tag{2.8}$$

so that the local $SU(3)$ gauge symmetry is maintained.

In order to solve the system numerically, the spacetime needs to be discretized. Suppose the discretized spacetime has lattice spacing a, then the gauge link variable $U_\mu(x)$ can be defined as

$$U_\mu(x) = e^{ig_0 a A_\mu(x+\frac{a}{2}\hat{\mu})}. \tag{2.9}$$

Under gauge transformation $\Lambda(x)$, $U_\mu(x)$ transforms as

$$U_\mu(x) \to \Lambda(x) U_\mu(x) \Lambda^{-1}(x+\hat{\mu}). \tag{2.10}$$

The gauge links also satisfy $U_\mu^\dagger(x) = U_{-\mu}(x+\hat{\mu})$, therefore the plaquette $U_{\mu\nu}(x)$ as shown below is gauge invariant,

$$U_{\mu\nu}(x) = \mathrm{Tr}\, U_\mu(x) U_\nu(x+\hat{\mu}) U_{-\mu}(x+\hat{\mu}+\hat{\nu}) U_{-\nu}(x+\hat{\nu}). \tag{2.11}$$

It can be shown that the gauge action in the following form has the right continuum limit when $a \to 0$,

$$S_G(U) = \frac{2N_c}{g_0^2} \sum_x \sum_{\mu,\nu,\mu>\nu} \mathrm{Tr}\left[1 - \frac{1}{2N_c}\left(U_{\mu\nu}(x) + U_{\mu\nu}^\dagger(x)\right)\right]. \tag{2.12}$$

Conventionally, we define $\beta = \frac{2N_c}{g_0^2}$.

The discretization of the fermion action is not so trivial. Naively, one could simply replace the derivative with a difference

$$\partial_\mu \psi(x) \to \frac{1}{2a}[\psi(x+\hat{\mu}) - \psi(x-\hat{\mu})], \tag{2.13}$$

and therefore the fermion action becomes

$$S_F(\psi, \bar{\psi}, U) = a^4 \sum_x \bar{\psi}(x) \left[\sum_\mu \frac{\gamma_\mu}{2a}\left[U_\mu(x)\psi(x+\bar{\mu}) - U_{-\mu}(x)\psi(x-\bar{\mu})\right] + m\psi(x)\right] \tag{2.14}$$

However, this possess a problem known as the "doubling problem", namely 15 unphysical modes would arise at the boundaries of the Brillouin zone because of the first order derivative. One way to solve this problem is by adding a second derivative to the action, which will vanish at the continuum limit,

$$aD_\mu^2 \psi(x) = a \sum_\mu \frac{1}{2a^2}\left[U_\mu(x)\psi(x+\hat{\mu}) - 2\psi(x) + U_{-\mu}(x)\psi(x-\hat{\mu})\right]. \tag{2.15}$$

Then the fermion action becomes

$$S_F = a^4 \sum_x \left\{\bar{\psi}(x)\left(m + \frac{4}{a}\right)\psi(x) - \bar{\psi}(x)\frac{1}{2a}\sum_\mu\left[(1-\gamma_\mu)U_\mu(x)\psi(x+\hat{\mu}) + (1+\gamma_\mu)U_{-\mu}(x)\psi(x-\hat{\mu})\right]\right\}, \tag{2.16}$$

or if we write in terms of Dirac operator $D(y,x)$,

$$D(y,x) = \left(m + \frac{4}{a}\right)\delta_{xy} - \frac{1}{2a}\sum_{\mu}\left[(1-\gamma_\mu)U_\mu(y)\delta_{y+\hat{\mu},x} + (1+\gamma_\mu)U_\mu(y)\delta_{y-\hat{\mu},x}\right], \quad (2.17)$$

$$S_F = a^4 \sum_{x,y} \bar{\psi}(y) D(y,x) \psi(x). \quad (2.18)$$

Conventionally, hopping parameter is defined as $\kappa = \frac{1}{2(am+4)}$. Note that this construction avoids the problem of doublers, but explicitly violates chiral symmetry.

2.2 Numerical methods

Even after we discretize the spacetime, it is still almost impossible to directly evaluate Eq. (2.4) because of the sheer amount of computation needed for the multi-dimensional integration. Therefore in reality the integral is approximated with Monte Carlo method.

Now let us consider a pure-gauge object

$$\langle O \rangle = \frac{1}{Z}\int \mathcal{D}U\, O(U) e^{-S_G(U)}, \qquad Z = \int \mathcal{D}U\, e^{-S_G(U)}. \quad (2.19)$$

In the Monte Carlo method, the integral is replaced by the average over the configuration space,

$$\langle O \rangle = \lim_{N\to\infty} \frac{1}{N}\sum_{i=1}^{N} O(U_i), \quad (2.20)$$

in which U_i are sampled in the configuration space according to probability distribution

$$dP(U) = \frac{1}{Z} e^{-S_G(U)} \mathcal{D}U. \quad (2.21)$$

In practice, N is usually a large finite number, and the error of $\langle O \rangle$ is of order $1/\sqrt{N}$. Samples U_i can be generated with algorithms such as Metropolis.

However if we include the fermion action, this approach fails. The reason is that the fermion fields anti-commute. This property is not captured in the usual Monte Carlo method described above. Luckily, this can be addressed by using Grassmann numbers for the fermion field. Consider Grassmann numbers η_i and η_j, then by definition, $\{\eta_i, \eta_j\} = 0$. One property of Grassmann number is that since $\eta_i^2 = 0$, a polynomial of Grassmann number is always truncated. Therefore a most general form of a polynomial involving 1 Grassmann variable is

$$a + a_1\eta.$$

For 2 Grassmann variables, a general polynomial has only four terms,

$$a + a_1\eta_1 + a_2\eta_2 + a_{12}\eta_1\eta_2.$$

Derivatives can be defined by

$$\frac{\partial 1}{\partial \eta_i} = 0, \quad \frac{\partial \eta_i}{\partial \eta_i} = 1, \quad \frac{\partial}{\partial \eta_i}\frac{\partial}{\partial \eta_j} = -\frac{\partial}{\partial \eta_j}\frac{\partial}{\partial \eta_i}, \quad \frac{\partial}{\partial \eta_i}\eta_j = -\eta_j\frac{\partial}{\partial \eta_i}.$$

For integration, a normalization condition is defined

$$\int d\eta_i 1 = 0, \quad \int d\eta_i \, \eta_i = 1.$$

Now suppose we apply a linear transformation on η with some matrix M, $\eta' = M\eta$, then

$$\begin{aligned}
&\int \mathcal{D}\eta \, \eta_1\eta_2\cdots\eta_N = \int \mathcal{D}\eta' \, \eta'_1\eta'_2\cdots\eta'_N \\
&= \int \mathcal{D}\eta' \sum_{i_1,\cdots i_N} M_{1i_1}\cdots M_{Ni_N}\eta_{i_1}\eta_{i_2}\cdots\eta_{i_N} \\
&= \int \mathcal{D}\eta' \sum_{i_1\cdots i_N} M_{1i_1}\cdots M_{Ni_N}\,\epsilon_{i_1 i_2\cdots i_N}\eta_1\eta_2\cdots\eta_N \\
&= \det M \int \mathcal{D}\eta' \, \eta_1\eta_2\cdots\eta_N,
\end{aligned} \tag{2.22}$$

in which $\epsilon_{i_1 i_2\cdots i_N}$ is the sign of permutation $i_1 i_2\cdots i_N$. Thus

$$\mathcal{D}\eta = \det M \, \mathcal{D}\eta'. \tag{2.23}$$

Now consider the following gaussian integral

$$Z_F = \int \mathcal{D}\eta\mathcal{D}\bar{\eta} \, e^{\bar{\eta}M\eta}, \tag{2.24}$$

in which M is a matrix. Again define $\eta' = M\eta$, using Eq. (2.22),

$$\begin{aligned}
Z_F &= \det M \int \mathcal{D}\eta'\mathcal{D}\bar{\eta} \, e^{\bar{\eta}\eta'} \\
&= \det M \prod_i \int d\eta'_i d\bar{\eta}_i \, e^{\bar{\eta}_i\eta'_i} \\
&= \det M \prod_i \int d\eta'_i d\bar{\eta}_i (1 + \bar{\eta}_i\eta'_i) \\
&= \det M.
\end{aligned} \tag{2.25}$$

Therefore, in order to include fermion action in Eq. (2.19), one may compute $\det(D)$, in which D is the Dirac operator, and evaluate

$$Z = \int \mathcal{D}U \, \det(D(U)) \, e^{-S_G(U)}, \tag{2.26}$$

using $\det(D(U)) \, e^{-S_G(U)}$ as Boltzmann factor.

In order to compute physical quantities, we need to know how to compute matrix element of operators. Suppose η, $\bar{\eta}$, θ, and $\bar{\theta}$ are all Grassmann variables. Define

$$W(\theta,\bar{\theta}) = \int \mathcal{D}\eta\mathcal{D}\bar{\eta}\, \exp\left(\bar{\eta}M\eta + \bar{\theta}\eta + \bar{\eta}\theta\right), \tag{2.27}$$

in which M is a matrix. Note that

$$\bar{\eta}M\eta + \bar{\theta}\eta + \bar{\eta}\theta = (\bar{\eta} + \bar{\theta}M^{-1})M(\eta + M^{-1}\theta) - \bar{\theta}M^{-1}\theta.$$

Define $\eta' = \eta + M^{-1}\theta$, $\bar{\eta}' = \bar{\eta} + \bar{\theta}M^{-1}$,

$$W(\theta,\bar{\theta}) = e^{-\bar{\theta}M^{-1}\theta}\int \mathcal{D}\eta'\mathcal{D}\bar{\eta}'\, e^{\bar{\eta}'M\eta'} = \det M\, e^{-\bar{\theta}M^{-1}\theta}. \tag{2.28}$$

Then to calculate any fermionic expectation values, one simply needs to take appropriate derivatives of W. For example,

$$\begin{aligned}
&\langle \eta_{i_1}\bar{\eta}_{j_1}\cdots\eta_{i_n}\bar{\eta}_{j_n}\rangle \\
&= \frac{1}{Z_F}\frac{\partial}{\partial\theta_{j_1}}\frac{\partial}{\partial\bar{\theta}_{i_1}}\cdots\frac{\partial}{\partial\theta_{j_n}}\frac{\partial}{\partial\bar{\theta}_{i_n}}W(\theta,\bar{\theta})\Big|_{\theta=\bar{\theta}=0} \\
&= (-1)^n \sum_{P(1,2,\ldots,n)} \epsilon_P (M^{-1})_{i_1 j_{P_1}} (M^{-1})_{i_2 j_{P_2}}\cdots(M^{-1})_{i_n j_{P_n}},
\end{aligned}$$

in which ϵ_P is the sign of permutation P. In practice, matrix M is replaced by the Dirac operator D. Therefore one can take the quark propagator D^{-1} as a basic building block of all fermionic correlation functions.

However, calculating D^{-1} on the lattice is not trivial, not only because matrix inversions are non-trivial to compute in general, but also the fact that the Dirac matrix is usually big. It is impractical to fully invert the Dirac matrix to produce the so-called "all-to-all" propagator. It is much more practical to calculate the propagator from a single point to all points,

$$D^{-1}(y,x_0) = \sum_x D^{-1}(y,x)S(x,x_0), \quad S(x,x_0) = \delta_{xx_0}. \tag{2.29}$$

Here S constraints the propagator to be from one point, x_0, and therefore is called a point source at x_0.

2.3 Overlap fermion

As shown in section 2.1, Wilson fermion explicitly violates chiral symmetry. This can be addressed by using more advanced fermion actions like overlap fermion and domain wall fermion.

In the continuum, if we perform a chiral rotation on the fermion fields,

$$\psi \to \psi' = e^{i\alpha\gamma_5}\psi, \quad \bar{\psi} \to \bar{\psi}' = \bar{\psi}e^{i\alpha\gamma_5},$$

it is easy to show that the massless lagrangian $L = \bar{\psi}\gamma_\mu D_\mu \psi$ is unchanged, because γ_μ anticommutes with γ_5. In other words, the Dirac operator D is chiral, if

$$D\gamma_5 + \gamma_5 D = 0. \tag{2.30}$$

In the continuum, $D = \gamma_\mu D_\mu$.

The lattice version of Eq. (2.30), as shown by Ginsparg and Wilson [2], is

$$D\gamma_5 + \gamma_5 D = D\gamma_5 D. \tag{2.31}$$

A solution of this equation has been found in the form of an overlap operator [3], defined by

$$D_{ov} = 1 + \gamma_5 \operatorname{sign}(H), \quad H = \gamma_5 D, \tag{2.32}$$

where D is some suitable kernel Dirac operator that is γ_5-hermitian, $\gamma_5 D \gamma_5 = D^\dagger$. Since H is hermitian, the matrix sign function is well-defined through the spectral theorem, therefore the overlap fermion is also γ_5-hermitian. Then

$$\begin{aligned} D_{ov} D_{ov}^\dagger &= (1 + \gamma_5 \operatorname{sign}(H))(1 + \operatorname{sign}(H)\gamma_5) \\ &= 1 + \gamma_5 \operatorname{sign}(H) + \operatorname{sign}(H)\gamma_5 + 1 + \gamma_5 \operatorname{sign}(H) \operatorname{sign}(H)\gamma_5 \\ &= 1 + \gamma_5 \operatorname{sign}(H) + \operatorname{sign}(H)\gamma_5 + 1 \\ &= D_{ov} + D_{ov}^\dagger. \end{aligned}$$

Thus, D_{ov} satisfies the Ginsparg-Wilson relation Eq. (2.31).

However, the sign function has proven to be nontrivial to evaluate. If one is to use the spectral theorem, the Wilson Dirac operator has to be diagonalized in order to extract the eigensystem. Computationally this is equivalent to a full inversion of the operator, and thus is impractical. In reality, the sign function is approximated through the Chebyshev polynomials [4], which are orthogonal polynomials $T_n(x)$ under the following inner product:

$$(f, g) = \int_{-1}^{1} dx \, \frac{f(x) g(x)}{\sqrt{1 - x^2}}.$$

Then a function $r(x)$ can be expanded as

$$r(x) = \sum_{n=0}^{\infty} c_n T_n(x) \approx \sum_{n=0}^{N-1} c_n T_n(x),$$

in which $c_n = (r, T_n)$. This expansion converges for functions that are continues in $[-1, 1]$. The coefficients can be approximated by

$$c_n = \frac{\pi}{N} \sum_{k=1}^{N} r(x_k) T_n(x_k), \quad x_k = \cos\left[\left(k - \frac{1}{2}\right)\frac{\pi}{N}\right]. \tag{2.33}$$

To calculate the sign function, we note that the sign function can also be written as $\text{sign}(H) = H/\sqrt{H^2}$. Suppose the eigenvalues of H^2 is bounded in domain $[\alpha^2, \beta^2]$, any values λ within this region can be mapped to variable $x \in [-1, 1]$ by

$$x = \frac{2\lambda - (\alpha^2 + \beta^2)}{\beta^2 - \alpha^2}.$$

Operator $1/\sqrt{H^2}$ can then be calculated through spectral theorem by calculating

$$r(x) = \frac{1}{\sqrt{\lambda}} = \left(\frac{1}{2}(\alpha^2 + \beta^2) + \frac{x}{2}(\beta^2 - \alpha^2)\right)^{-\frac{1}{2}}.$$

Coefficients c_n can then be calculated with Eq. (2.33). The sign function is then

$$\text{sign}(H) = \frac{H}{\sqrt{H^2}} \approx H \sum_{n=0}^{N-1} c_n T_n(X), \quad X = \frac{2H^2 - (\alpha^2 + \beta^2)}{\beta^2 - \alpha^2}. \tag{2.34}$$

Chapter 3

Correlation functions

3.1 Nucleon two-point correlation functions

For free spin-$\frac{1}{2}$ particles, the equations of motion are

$$\begin{cases} (\not{p} - im)u(p,s) = 0 \\ \bar{u}(p,s)(\not{p} - im) = 0. \end{cases} \tag{3.1}$$

Therefore

$$\begin{aligned} u(p,s) &= \sqrt{\frac{E_p + m}{2m}} \begin{pmatrix} I \\ -i\frac{\vec{\sigma}\cdot\vec{p}}{E_p+m} \end{pmatrix} \chi_s \\ \bar{u}(p,s) &= \sqrt{\frac{E_p + m}{2m}} \chi_s^\dagger \begin{pmatrix} I \\ -i\frac{\vec{\sigma}\cdot\vec{p}}{E_p+m} \end{pmatrix}^T, \end{aligned} \tag{3.2}$$

$$\bar{u}(p,s)u(p,s') = \delta_{ss'}, \quad \sum_s u(p,s)\bar{u}(p,s) = \frac{-i\not{p} + m}{2m} \tag{3.3}$$

Consider the nucleon state with principle quantum number n, momentum $\vec{p}$, and spin s. Normalization on the continuum is defined as

$$\sum_{n,s} \int \frac{d^3\vec{p}}{(2\pi)^3} \frac{m}{E_{\vec{p}}} |n\vec{p}s\rangle\langle n\vec{p}s| = 1.$$

The coupling strength λ_n can be defined via

$$\begin{aligned}
\langle 0|\chi(0)|n_+\vec{p}s\rangle &= \lambda_n^+\sqrt{\frac{m_n^+}{E_n^+}}u_n^+(\vec{p},s)\\
\langle n_+\vec{p}s|\bar{\chi}(0)|0\rangle &= \bar{\lambda}_n^+\sqrt{\frac{m_n^+}{E_n^+}}\bar{u}_n^+(\vec{p},s)\\
\langle 0|\chi(0)|n_-\vec{p}s\rangle &= \lambda_n^-\sqrt{\frac{m_n^-}{E_n^-}}\gamma_5 u_n^-(\vec{p},s)\\
\langle n_-\vec{p}s|\bar{\chi}(0)|0\rangle &= -\bar{\lambda}_n^-\sqrt{\frac{m_n^-}{E_n^-}}\bar{u}_n^-(\vec{p},s)\gamma_5,
\end{aligned}$$

where I have used $m_n^\pm$ and $E_n^\pm$ to denote the mass and energy of the nth states with even/odd parity. However on the lattice, the normalization is taken to be

$$\sum_{n,\vec{p},s}|n\vec{p}s\rangle\langle n\vec{p}s| = 1. \tag{3.4}$$

And if one replaces $\int\frac{d^3\vec{p}}{(2\pi)^3}$ with $\frac{1}{V}\sum_{\vec{p}}$ to go from continuum to the discrete lattice, where $V = a^3N$, and N is the number of lattice sites in one time slice, it naturally follows that

$$|n\vec{p}s\rangle_L = \sqrt{\frac{m}{VE_{\vec{p}}}}\,|n\vec{p}s\rangle_C, \tag{3.5}$$

where I have used subscripts C and L to denote continuum and lattice quantities, respectively. Also it is conventional to let $\psi_L = a^{\frac{3}{2}}\psi_C$ for fermion field ψ, in order to make it dimension-less on the lattice. Then on the lattice

$$\begin{aligned}
\langle 0|\chi(0)|n_+\vec{p}s\rangle &= a^3\lambda_n^+\sqrt{\frac{m_n^+}{NE_n^+}}u_n^+(\vec{p},s)\\
\langle n_+\vec{p}s|\bar{\chi}(0)|0\rangle &= a^3\bar{\lambda}_n^+\sqrt{\frac{m_n^+}{NE_n^+}}\bar{u}_n^+(\vec{p},s)\\
\langle 0|\chi(0)|n_-\vec{p}s\rangle &= a^3\lambda_n^-\sqrt{\frac{m_n^-}{NE_n^-}}\gamma_5 u_n^-(\vec{p},s)\\
\langle n_-\vec{p}s|\bar{\chi}(0)|0\rangle &= -a^3\bar{\lambda}_n^-\sqrt{\frac{m_n^-}{NE_n^-}}\bar{u}_n^-(\vec{p},s)\gamma_5,
\end{aligned} \tag{3.6}$$

In order to calculate nucleon properties, we need an object $\bar{\chi}$ to create a nucleon state at some initial point, and another object χ to annihilate the state at some other point. In lattice QCD, these objects are called interpolators. For proton, the interpolator is usually taken to be

$$\chi(x) = \epsilon_{abc}u(x)_a[u(x)_b^T C\gamma_5 d(x)_c], \tag{3.7}$$

in which $u(x)$ and $d(x)$ are quark fields for u and d quark respectively, and C is the charge conjugation operator. Indices a, b, and c are for the color, and the Levi-Civita symbol is presented to make the proton color-singlet. The gamma structure is to make sure the state has the correct intrinsic quantum numbers. In this interpolator, $u(x)^T C\gamma_5 d(x)$ has isospin $I = 0$ and spin $J = 0$, therefore χ has $I = 1/2$, $I_z = +1/2$ and $J = 1/2$.

Define the nucleon two-point function as

$$G_{NN}(\vec{p}, t) = \sum_{\vec{x}} e^{-i\vec{p}\cdot\vec{x}} \langle 0|\chi(x)\bar{\chi}(0)|0\rangle. \tag{3.8}$$

Insert complete energy eigenstates with principle quantum number n, momentum q and spin s,

$$\begin{aligned}
&G_{NN}(\vec{p}, t) \\
&= \sum_{\vec{x}} e^{-i\vec{p}\cdot\vec{x}} \sum_{n,q,s} \langle 0|e^{Ht} e^{-i\vec{q}\cdot\vec{x}} \chi(0) e^{-Ht} e^{i\vec{q}\cdot\vec{x}} |n\vec{q}s\rangle\langle n\vec{q}s|\bar{\chi}(0)|0\rangle \\
&= \sum_{\vec{x}} e^{-i\vec{p}\cdot\vec{x}} \sum_{n} \sum_{s} e^{-E_n t} e^{i\vec{q}\cdot\vec{x}} \langle 0|\chi(0)|n\vec{q}s\rangle\langle n\vec{q}s|\bar{\chi}(0)|0\rangle \\
&= N \sum_{n,\vec{q},s} \delta_{\vec{p}\vec{q}} e^{-E_n t} e^{i\vec{q}\cdot\vec{x}} \langle 0|\chi(0)|n\vec{q}s\rangle\langle n\vec{q}s|\bar{\chi}(0)|0\rangle \\
&= N \sum_{n,s} e^{-E_n(\vec{p})t} e^{i\vec{p}\cdot\vec{x}} \langle 0|\chi(0)|n\vec{p}s\rangle\langle n\vec{p}s|\bar{\chi}(0)|0\rangle
\end{aligned} \tag{3.9}$$

where $E_n(\vec{p}) = \sqrt{m_n^2 + \vec{p}^2}$. Use Eq. (3.3), and split the even parity from the odd parity part,

$$\begin{aligned}
G_{NN}(\vec{p}, t) = a^6 \Bigg(&\sum_{n_+} \lambda_n^+ \bar{\lambda}_n^+ e^{-E_n^+(\vec{p})t} \frac{m_n^+}{E_n^+} \frac{-i\not{p} + m_n^+}{2m_n^+} \\
&+ \sum_{n_-} \lambda_n^- \bar{\lambda}_n^- e^{-E_n^-(\vec{p})t} \frac{m_n^-}{E_n^-} \frac{i\not{p} + m_n^-}{2m_n^-} \Bigg).
\end{aligned}$$

In practice, one usually desire the correlation function with definite parity. Define parity projection operator $P_\pm = (1 \pm \gamma_4)/2$, and use

$$\mathrm{Tr}\left(-i\not{p} + m\right) = 4m, \quad \mathrm{Tr}\left[\gamma_4(-i\not{p} + m)\right] = -4ip_4 = 4E_p, \tag{3.10}$$

then

$$\begin{aligned}
\mathrm{Tr}[P_+ G_{NN}(\vec{p}, t)] = a^6 \Bigg(&\sum_{n_+} \lambda_n^+ \bar{\lambda}_n^+ e^{-E_n^+ t} \frac{m_n^+}{E_n^+} \frac{E_n^+ + m_n^+}{m_n^+} \\
&- \sum_{n_-} \lambda_n^- \bar{\lambda}_n^- e^{-E_n^- t} \frac{m_n^-}{E_n^-} \frac{E_n^- - m_n^-}{m_n^-} \Bigg).
\end{aligned}$$

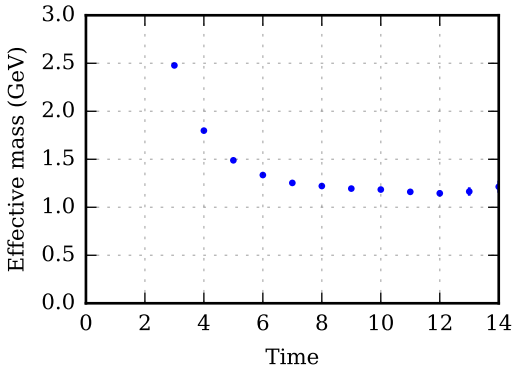

Figure 3.1: Effective mass plotted as a function of time. Overlap fermion is used on top of a RBC/UKQCD domain wall emsemble, with $2+1$ flavors, $a = 0.112(3)$ fm, $m_\pi = 330$ MeV. Inversion is done on a point source.

For zero momentum, $E_n \to m_n$, the odd parity part vanishes, only even parity survives,

$$\mathrm{Tr}[P_+ G_{NN}(\vec{p}=0,t)] \to a^6 \sum_{n_+} \lambda_n^+ \bar{\lambda}_n^+ e^{-E_n^+ t} \frac{m_n^+}{m_n^+} \left(1 + \frac{m_n^+}{m_n^+}\right). \tag{3.11}$$

If we sort the masses of all states as $m_0 < m_1 < \cdots$, as t goes large, the lowest state dominates the exponential, therefore

$$\mathrm{Tr}[P_+ G_{NN}(\vec{p}=0,t)] \to a^6 \lambda_0^+ \bar{\lambda}_0^+ e^{-E_0^+ t} \frac{m_0^+}{m_0^+} \left(1 + \frac{m_0^+}{m_0^+}\right) = 2a^6 \lambda_0^+ \bar{\lambda}_0^+ e^{-m_0^+ t}, \quad t \to \infty. \tag{3.12}$$

Conventionally, effective mass is defined on the lattice as

$$m_{\mathrm{eff}} = \log \frac{\mathrm{Tr}[P_+ G_{NN}(\vec{p}\to 0,t)]}{\mathrm{Tr}[P_+ G_{NN}(\vec{p}\to 0,t+1)]} \to m_0^+, \quad t \to \infty. \tag{3.13}$$

In this case, m_0^+ is the mass of the proton. If we plot m_{eff} as a function of t, we can see that at large t, it approaches a constant number. Figure 3.1 shows a typical effective mass plot. It is evident that at small t, contributions from excited states brings the effective mass high; however as t gets big, effective mass forms a plateau.

With the help of interpolators, we can calculate nucleon correlation function. However on the lattice, we don't have access to quark fields; the most basic object we can calculate is a quark propagator. Therefore we need to express the correlation function in terms of quark propagators. To do that, let us write down the proton interpolator in a general way, with different diquark structures.

$$\begin{aligned} \chi_\delta(x) &= \epsilon_{abc}[(u^T)^a_\alpha(x)(\Gamma_1)_{\alpha\beta} d^b_\beta(x)](\Gamma_2)_{\delta\gamma} u^c_\gamma(x), \\ \bar{\chi}_\delta(x) &= -\epsilon_{abc} \bar{u}^c_\gamma(x)(\Gamma_2')_{\delta\gamma}[\bar{d}^b_\beta(x)(\Gamma_1')_{\alpha\beta}(\bar{u}^T)^a_\alpha(x)], \end{aligned} \tag{3.14}$$

in which Greek indices are in dirac space, while Latin indices are in color space; the Γ-s are combinations of γ-matrices. If we set $\Gamma_1 = \Gamma_1' = C\gamma_5$, and $\Gamma_2 = \Gamma_2' = 1$, then we get Eq. (3.7).

Now consider a correlation function projected to a definite parity,

$$\begin{aligned}\langle P_{\pm}\chi(y)\bar{\chi}(x)\rangle &= \langle P^{\pm}_{\delta'\delta}\epsilon_{abc}[(u^T)^a_\alpha(y)(\Gamma_1)_{\alpha\beta}d^b_\beta(y)](\Gamma_2)_{\delta\gamma}u^c_\gamma(y)\\ &\quad \epsilon_{a'b'c'}\bar{u}^{c'}_{\gamma'}(x)(\Gamma_2')_{\delta'\gamma'}[\bar{d}^{b'}_{\beta'}(x)(\Gamma_1')_{\alpha'\beta'}(\bar{u}^T)^{a'}_{\alpha'}(x)]\rangle\\ &= \langle P^{\pm}_{\delta'\delta}\epsilon_{abc}\epsilon_{a'b'c'}(\Gamma_1)_{\alpha\beta}(\Gamma_2)_{\delta\gamma}(\Gamma_1')_{\alpha'\beta'}(\Gamma_2')_{\delta'\gamma'}\\ &\quad (u^T)^a_\alpha(y)u^c_\gamma(y)\bar{u}^{c'}_{\gamma'}(x)(\bar{u}^T)^{a'}_{\alpha'}(x)d^b_\beta(y)\bar{d}^{b'}_{\beta'}(x)\rangle.\end{aligned} \tag{3.15}$$

Now we can contract quark fields into quark propagators. Since there are two pairs of u fields, there are 2 kinds of contractions.

$$\begin{aligned}&\langle P_{\pm}\chi(y)\bar{\chi}(x)\rangle\\ &= \langle P^{\pm}_{\delta'\delta}\epsilon_{abc}\epsilon_{a'b'c'}(\Gamma_1)_{\alpha\beta}(\Gamma_2)_{\delta\gamma}(\Gamma_1')_{\alpha'\beta'}(\Gamma_2')_{\delta'\gamma'}\\ &\quad \Big[G^{(u)aa'}_{\alpha\alpha'}(y,x)G^{(d)bb'}_{\beta\beta'}(y,x)G^{(u)cc'}_{\gamma\gamma'}(y,x)\\ &\quad -G^{(u)ac'}_{\alpha\gamma'}(y,x)G^{(d)bb'}_{\beta\beta'}(y,x)G^{(u)ca'}_{\gamma\alpha'}(y,x)\Big]\rangle,\end{aligned} \tag{3.16}$$

in which $G^{(u)ba}_{\beta\alpha}(y,x)$ denotes a quark propagator of flavor u from position x, color a, and Dirac index α, to position y, color b, and Dirac index β. For clarity, let us ignore color indices and spacetime coordinates, and write this expression in matrix notation in Dirac space. The first term becomes

$$\begin{aligned}&\mathrm{Tr}\left[P_\pm\left(\Gamma_2 G_{(u)}(\Gamma_2')^T\right)^T\right]\mathrm{Tr}\left[\Gamma_1'(G^T_{(u)}\Gamma_1 G_{(d)})^T\right]\\ =\ &\mathrm{Tr}\left(P_\pm\Gamma_2'G^T_{(u)}\Gamma_2^T\right)\mathrm{Tr}\left(\Gamma_1'G^T_{(d)}\Gamma_1^T G_{(u)}\right).\end{aligned}$$

The second term becomes

$$\begin{aligned}&-\mathrm{Tr}\left[\left(\Gamma_2'\left(\left(\left(\left(\Gamma_1^T G_{(u)}\right)^T G_{(d)}\right)(\Gamma_1')^T\right)G^T_{(u)}\right)\Gamma_2^T\right)\right]\\ =\ &-\mathrm{Tr}\left[P_\pm\Gamma_2'\left(\Gamma_2 G_{(u)}\Gamma_1' G_{(d)}\Gamma_1^T G_{(u)}\right)^T\right].\end{aligned}$$

If we project to zero momentum, and use point source at $t=0$, then there's no spatial dependence in the correlation function,

$$\begin{aligned}&\mathrm{Tr}[P_\pm G_{NN}(t,0)]\\ =&\sum_{\vec{x}}\langle P_\pm\chi(x)\bar{\chi}(0)\rangle\\ =&\sum_{\vec{x}}\Big\langle\mathrm{Tr}\left(P_\pm\Gamma_2'G^T_{(u)}\Gamma_2^T\right)\mathrm{Tr}\left(\Gamma_1'G^T_{(d)}\Gamma_1^T G_{(u)}\right)\\ &-\mathrm{Tr}\left[P_\pm\Gamma_2'\left(\Gamma_2 G_{(u)}\Gamma_1' G_{(d)}\Gamma_1^T G_{(u)}\right)^T\right]\Big\rangle\end{aligned} \tag{3.17}$$

3.2 Three-point correlation functions

Three-point correlation functions can also be constructed on the lattice. For any operator O in general, the three-point function is

$$G_{NON}(t_2, t_1, \vec{p}_f, \vec{p}_i) = \sum_{x_1, x_2} e^{-i\vec{p}_f\cdot(\vec{x}_2-\vec{x}_1)} e^{-i\vec{p}_i\cdot(\vec{x}_1-\vec{x}_0)} \langle 0|T(\chi(x_2)O(x_1)\bar{\chi}(x_0))|0\rangle, \tag{3.18}$$

in which t_1 is the insertion time, and t_2 is the sink time. We are only interested in forward scattering case, so we may set $\vec{p}_i = \vec{p}_f = \vec{p}$, and rewrite G_{NON} as

$$G_{NON}(t_2, t_1, \vec{p}_f, \vec{p}_i) = \sum_{x_2, x_1} e^{-i\vec{p}\cdot(\vec{x}_2-\vec{x}_0)} \langle 0|T(\chi(x_2)O(x_1)\bar{\chi}(x_0))|0\rangle. \tag{3.19}$$

If we insert a complete energy eigenstate, and note that

$$\begin{aligned} \langle 0|O(x)|n\rangle &= \langle 0|e^{H(t-t_0)} e^{-i\vec{p}(\vec{x}-\vec{x}_0)} O(x_0) e^{-H(t-t_0)} e^{i\vec{p}(\vec{x}-\vec{x}_0)} n\rangle \\ &= e^{-E_p(t-t_0)} e^{i\vec{p}(\vec{x}-\vec{x}_0)} \langle 0|O(x_0)|n\rangle, \end{aligned} \tag{3.20}$$

G_{NON} becomes

$$\begin{aligned} & G_{NON}(t_2, t_1, \vec{p}) \\ &= \sum_{x_2, x_1} e^{-i\vec{p}\cdot(\vec{x}_2-\vec{x}_0)} \sum_{\substack{n_1\vec{q}_1 s_1 \\ n_2\vec{q}_2 s_2}} e^{-E_2(t_2-t_1)} e^{-E_1(t_1-t_0)} \langle 0|\chi(x_2)|n_2\vec{q}_2 s_2\rangle \langle n_2\vec{q}_2 s_2|O(x_1)|n_1\vec{q}_1 s_1\rangle \langle n_1\vec{q}_1 s_1|\bar{\chi}(x_0)|0\rangle \\ &= \sum_{x_2, x_1} e^{-i\vec{p}\cdot(\vec{x}_2-\vec{x}_0)} \sum_{\substack{n_1\vec{q}_1 s_1 \\ n_2\vec{q}_2 s_2}} e^{-E_2(t_2-t_1)} e^{-E_1(t_1-t_0)} \phi \langle 0|\chi(x_0)|n_2\vec{q}_2 s_2\rangle \langle n_2\vec{q}_2 s_2|O(x_0)|n_1\vec{q}_1 s_1\rangle \langle n_1\vec{q}_1 s_1|\bar{\chi}(x_0)|0\rangle, \end{aligned} \tag{3.21}$$

where

$$\begin{aligned} \phi =& e^{-E_2(t_2-t_0)} e^{i\vec{q}_2\cdot(\vec{x}_2-\vec{x}_0)} e^{E_2(t_1-t_0)} e^{-i\vec{q}_2\cdot(\vec{x}_1-\vec{x}_0)} \\ & e^{-E_1(t_1-t_0)} e^{i\vec{q}_1\cdot(\vec{x}_1-\vec{x}_0)} e^{E_1(t_1-t_0)} e^{-i\vec{q}_1\cdot(\vec{x}_1-\vec{x}_0)}. \end{aligned} \tag{3.22}$$

Evaluating the sum over $\vec{x}_1$ and $\vec{x}_2$, one gets

$$\begin{aligned} & G_{NON}(t_2, t_1, \vec{p}) \\ &= N^2 \sum_{\substack{n_1\vec{q}_1 s_1 \\ n_2\vec{q}_2 s_2}} e^{-E_2(t_2-t_1)} e^{-E_1(t_1-t_0)} \delta_{\vec{p}\vec{q}_2} \delta_{\vec{q}_1\vec{q}_2} e^{-E_2(t_2-t_0)} e^{E_2(t_1-t_0)} e^{-E_1(t_1-t_0)} e^{E_1(t_1-t_0)} e^{-i\vec{q}_1\cdot(\vec{x}_1-\vec{x}_0)} \\ & \langle 0|\chi(x_0)|n_2\vec{q}_2 s_2\rangle \langle n_2\vec{q}_2 s_2|O(x_0)|n_1\vec{q}_1 s_1\rangle \langle n_1\vec{q}_1 s_1|\bar{\chi}(x_0)|0\rangle \\ &= N^2 \sum_{\substack{n_1 s_1 \\ n_2 s_2}} e^{-E_2(t_2-t_1)} e^{-E_1(t_1-t_0)} \langle 0|\chi(x_0)|n_2\vec{p}s_2\rangle \langle n_2\vec{p}s_2|O(x_0)|n_1\vec{p}s_1\rangle \\ & \langle n_1\vec{p}s_1|\bar{\chi}(x_0)|0\rangle. \end{aligned} \tag{3.23}$$

For forward scattering, set $s_1 = s_2 = s$, and rewrite

$$G_{NON}(t_2, t_1, \vec{p}) = N^2 \sum_{n_1 n_2 s} e^{-E_2(t_2-t_1)} e^{-E_1(t_1-t_0)} \langle 0|\chi(x_0)|n_2\vec{p}s\rangle\langle n_2\vec{p}s|O(x_0)|n_1\vec{p}s\rangle\langle n_1\vec{p}s|\bar{\chi}(x_0)|0\rangle. \tag{3.24}$$

If we let $t_2 \gg t_1 \gg t_0$, then only the ground state survives the exponentials,

$$\begin{aligned} &G_{NON}(t_2, t_1, \vec{p}) \\ \to\ & N^2 \sum_s \Big(e^{-E_0^+(t_2-t_0)} \langle 0|\chi(x_0)|0^+\vec{p}s\rangle\langle 0^+\vec{p}s|O(x_0)|0^+\vec{p}s\rangle\langle 0^+\vec{p}s|\bar{\chi}(x_0)|0\rangle \\ &\quad + e^{-E_0^-(t_2-t_0)} \langle 0|\chi(x_0)|0^-\vec{p}s\rangle\langle 0^-\vec{p}s|O(x_0)|0^-\vec{p}s\rangle\langle 0^-\vec{p}s|\bar{\chi}(x_0)|0\rangle \Big) \end{aligned} \tag{3.25}$$

Use Eq. (3.6),

$$\begin{aligned} &G_{NON}(t_2, t_1, \vec{p}) \\ \to\ & Na^6 \Bigg(e^{-E_0^+(t_2-t_0)} \langle 0^+\vec{p}s|O(x_0)|0^+\vec{p}s\rangle\, |\lambda^+|^2 \frac{m^+}{E^+} \sum_s u^+(\vec{p}, s)\bar{u}^+(\vec{p}, s) \\ &+ e^{-E_0^-(t_2-t_0)} \langle 0^-\vec{p}s|O(x_0)|0^-\vec{p}s\rangle\, |\lambda^-|^2 \frac{m^-}{E^-} \sum_s \gamma_5 u^-(\vec{p}, s)\bar{u}^-(\vec{p}, s)\gamma_5 \Bigg), \end{aligned} \tag{3.26}$$

If we project this three-point function to positive parity by multiplying $P_+ = (1+\gamma_4)/2$, and use Eq. (3.3) and Eq. (3.10), we get

$$\begin{aligned} &\mathrm{Tr}(P_+ G_{NON}(t_2, \vec{p})) \\ \to\ & Na^6 \Bigg[e^{-E_0^+(t_2-t_0)} \sum_s \langle 0^+\vec{p}s|O(x_0)|0^+\vec{p}s\rangle\, |\lambda^+|^2 \frac{m^+}{E^+} \left(1 + \frac{E^+}{m^+}\right) \\ &+ e^{-E_0^-(t_2-t_0)} \sum_s \langle 0^-\vec{p}s|O(x_0)|0^-\vec{p}s\rangle\, |\lambda^-|^2 \frac{m^-}{E^-} \left(1 - \frac{E^-}{m^-}\right) \Bigg]. \end{aligned} \tag{3.27}$$

For small momentum, $E \approx m$. Also notice that $E_0^- > E_0^+$ and therefore the exponential factor $e^{-E_0^-(t_2-t_0)}$ is much smaller than the corresponding positive parity factor, when $t_2 - t_0$ is large. Thus the negative parity contribution becomes negligible, we can ignore the $+$ superscripts.

$$\mathrm{Tr}(P_+ G_{NON}(t_2, \vec{p})) \to Na^6 e^{-E_0(t_2-t_0)} \sum_s \langle 0\vec{p}s|O(x_0)|0\vec{p}s\rangle\, |\lambda|^2 \frac{m}{E} \left(1 + \frac{E}{m}\right). \tag{3.28}$$

In terms of quark fields, consider having a nucleon two-point function, and insert a general operator in the form of $O = \bar{\psi}\Gamma\psi$, in which ψ and $\bar{\psi}$ are quark fields. Using Eq. (3.7), also similarly to Eq. (3.15), one can have

$$\begin{aligned} &\langle \chi_{\alpha'}(x) O(y) \bar{\chi}_\alpha(0)\rangle \\ =\ & \sum_{\substack{a,b,c \\ a',b',c'}} \Big\langle d^{b'}_{\beta'}(x)(\Gamma_2)_{\beta'\gamma'} u^{c'}_{\gamma'}(x)(\Gamma_1)_{\alpha'\delta'} u^{a'}_{\delta'}(x)\, \bar{\psi}^d_\rho(y)\Gamma_{\rho\rho'}\psi^{d'}_{\rho'}(y) \\ &\bar{u}^a_\delta(0)(\bar{\Gamma}_1)_{\delta\alpha}\bar{u}^c_\gamma(0)(\bar{\Gamma}_2)_{\gamma\beta}\bar{d}^b_\beta(0)\epsilon^{abc}\epsilon^{a'b'c'}\Big\rangle. \end{aligned} \tag{3.29}$$

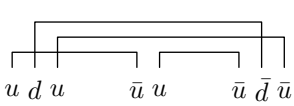

(a) Example of connected insertions

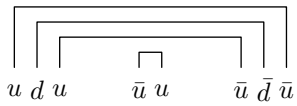

(b) Example of disconnected insertion

Figure 3.2: Illustrations of different ways of three-point function contractions. The udu and $\bar{u}\bar{d}\bar{u}$ denote proton interpolation fields, and $\bar{u}u$ in the middle denotes current insertion.

Depending on the flavor of ψ, there can be different ways of contraction. For example if ψ are u quarks, it can contract with the u quarks in the proton interpolation fields, and result in

$$\langle \chi(x)O(y)\bar{\chi}(0)\rangle = \left\langle \Gamma_1 G^{(u)}(x,0)\bar{\Gamma}_2 \left[G^{(d)}(x,0)\right]^T \Gamma_2 G^{(u)}(x,y)\Gamma G^{(u)}(y,0)\bar{\Gamma}_1 \right\rangle . \tag{3.30}$$

This is one of the "connected insertions" shown in Figure 3.2a. The quark fields in the current can also contract with themselves, as shown in Figure 3.2b. This is the "disconnected insertion", in which the three-point function is simply a product of proton two-point function and the loop,

$$\begin{aligned} &\mathrm{Tr}\langle P_\pm \chi(x)O(y)\bar{\chi}(0)\rangle \\ =& \left\langle \left\{ \mathrm{Tr}\left(P_\pm \Gamma_2' G^T_{(u)}(x,0)\Gamma_2^T\right) \mathrm{Tr}\left(\Gamma_1' G^T_{(d)}(x,0)\Gamma_1^T G_{(u)}(x,0)\right) \right.\right. \\ &\left.\left. - \mathrm{Tr}\left[P_\pm \Gamma_2' \left(\Gamma_2 G_{(u)}(x,0)\Gamma_1' G_{(d)}(x,0)\Gamma_1^T G_{(u)}(x,0)\right)^T\right] \right\} \mathrm{Tr}\left[\Gamma G_{(u)}(y,y)\right] \right\rangle \end{aligned} \tag{3.31}$$

Obviously, if the current has heavy flavors, only the disconnected insertion contributes to the matrix element.

Chapter 4

Numerical Techniques

4.1 Extended quark sources

As mentioned in section 2.2, propagators are calculated from quark sources. Point sources are the simplest quark sources one can have, and not necessarily the most useful. As shown in Figure 3.1, excited states contribute significantly at small t, which is not ideal if we want to calculate hadron properties. In principle, we would like the nucleon plateau in the effective mass plot to be as long as possible. This is usually achieved by using a smeared source [5].

Consider a quark source

$$\eta_S(x') = S(x', x)\eta(x), \tag{4.1}$$

where η_S is the smeared source. By design, $S(x', x)$ produces a gaussian distribution with a Klein-Gordon propagator. It is computed by repeating an iteration n times, so that [6]

$$S(x', x) = \left(1 - \frac{3w}{2n}\right)^n \left[1 + \frac{w^2}{4n - 6w^2} \sum_{i=1}^{3} \left(U_i(x', t)\delta_{x', x-\hat{i}} + U_i(x' - \hat{i}, t)\delta_{x', x+\hat{i}}\right)\right]^n.$$

The coefficients are designed so that w would be approximately the "size" of the smeared source. If we define the radius to be

$$r = \sqrt{\frac{\sum_x x^2 \rho(x)}{\sum_x \rho(x)}}, \tag{4.2}$$

where $\rho(x)$ is the norm of the source at x. Then as shown in Figure 4.1 r increases with w

Smearing is known to make the signal of the ground state stronger in the nucleon 2-point function. As shown in Figure 4.2, the nucleon is enhanced with a bigger smear size, which results in a flatter effective mass, and in turn giving a longer nucleon plateau to fit. This is most desirable if nucleon properties are of interests.

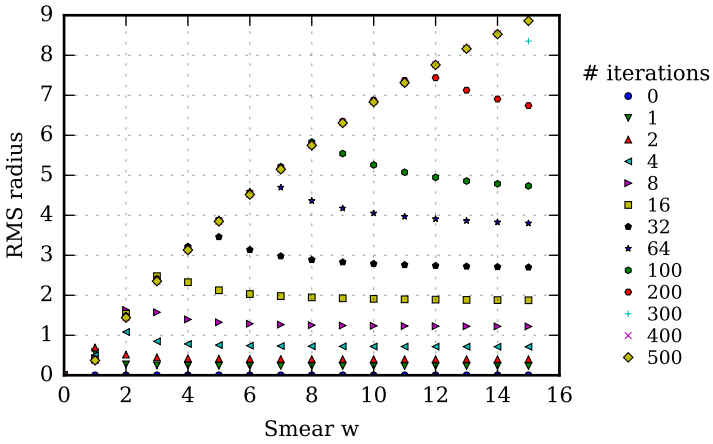

Figure 4.1: Smear size for different parameters.

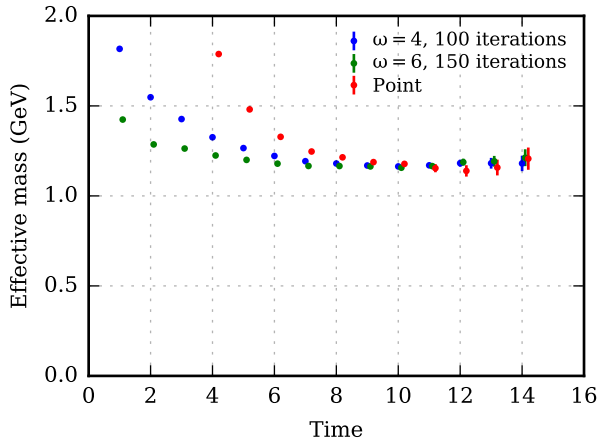

Figure 4.2: Effective mass from sources with various size. Inversion is done on RBC/UKQCD's $24^3 \times 64$ domain wall lattice with $m_\pi \approx 330\,\mathrm{MeV}$.

4.2 Grid source with Z_3 noises

So far we have considered quark source with a single (smeared) point. A natural next step is to look into source with multiple points; specifically, a simple case would be where the source points are arranged in a grid on the source time slice. Ideally, such a source would provide more statistics and small error, because it covers a larger subspace in the whole propagator space. However, this is not the case if one actually inverts such a grid source.

The reason is shown in Figure 4.3. When using a grid source, three propagators are contracted to form a 2-point function. However the three propagators do not necessarily comes from the same source point (illustrated by the red lines in the figure). Without any quark lines to connect different source points, the 2-point function is not gauge-invariant, and therefore is noisy.

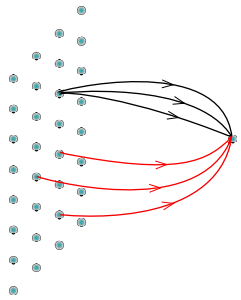

Figure 4.3: Illustration of quark lines with grid source. The red lines are not gauge-invariant, while the black lines are.

To make sure the propagators in a 2-point function comes from the same point, a stochastic technique can be applied [7]. Consider an ensemble of random variables $\theta(x)$ distributed on the lattice with the following properties

$$\theta(x)^3 = 1, \quad \langle \theta(x)\theta(y)\theta(z) \rangle = \delta_{xy}\delta_{yz}, \tag{4.3}$$

in which the angular bracket denotes expectation value over the noise ensemble. As shown in Eq. (3.16), the 2-point function of nucleon can be writting as a linear function of three quark propagators

$$\begin{aligned} \langle P_{\pm}\chi(y)\bar{\chi}(x) \rangle &= \left\langle G_{NN} \left(\sum_i \theta_i G_i, \sum_j \theta_j G_j, \sum_k \theta_k G_k \right) \right\rangle \\ &= \sum_{i,j,k} \langle \theta_i\theta_j\theta_k G_{NN} \left(G_i, G_j, G_k \right) \rangle , \end{aligned} \tag{4.4}$$

in which i, j, and k labels the source grid points. Use Eq. (4.3) and evaluate the summations over j and k,

$$\langle P_{\pm}\chi(y)\bar{\chi}(x) \rangle = \sum_i \langle G_{NN} \left(G_i, G_i, G_i \right) \rangle . \tag{4.5}$$

Thus the stochastic noises force the three propagators to come from the same source point, and avoid the gauge invariance problem. In practice, random numbers from the Z_3 group has been found to satisfy Eq. (4.3), and work well. [8]

4.3 Lowmode substitution

However, it is found that adding Z_3 noises is not enough in order to use the grid source effectively. A technique called lowmode substitution must be applied along with it. Define the massive overlap operator as

$$\begin{aligned} D(m, \rho) &= \rho D_{ov}(\rho) + m \left(1 - \frac{D_{ov}(\rho)}{2} \right) \\ &= \rho + \frac{m}{2} + \left(\rho - \frac{m}{2} \right) \gamma_5 \, \mathrm{sign}(H), \end{aligned} \tag{4.6}$$

in which $\rho = 4 - 1/(2\kappa)$, and κ is the hopping parameter for the Wilson kernel. If we replace the quark field with $\psi' = (1 - \frac{D_{ov}}{2})\psi$ in correlation functions, for example, Eq. (3.15), we arrive at the so-called effective propagator D_{eff}^{-1} [9, 10], which has the same factor,

$$G = D_{eff}^{-1} = \left(1 - \frac{D_{ov}}{2}\right) D_m^{-1} = \frac{1}{D_c + m}, \tag{4.7}$$

in which

$$D_c = \frac{\rho D_{ov}}{1 - \frac{D_{ov}}{2}} \tag{4.8}$$

is chiral, $\{\gamma_5, D_c\} = 0$. Suppose D_{ov} has eigenvectors $|i\rangle$ and eigenvalues λ_i, then

$$D(m, \rho)|i\rangle = \left[\rho\lambda_i + m\left(1 - \frac{\lambda_i}{2}\right)\right]|i\rangle. \tag{4.9}$$

It is possible to separate the propagator into low-mode part and high-mode part, by defining the low-mode source η^L and high-mode source η^H as

$$\eta^L = \sum_i^n |i\rangle\langle i|\eta\rangle, \quad \eta^H = \eta - \eta^L,$$

in which i goes from the lowest-lying mode to some cutoff n. Also notice that the eigenvalues of D_{ov} come in pairs of conjugate numbers, with associated eigenvectors $|i\rangle$ and $\gamma_5|i\rangle$ [8],

$$D_{ov}|i\rangle = \lambda_i|i\rangle, \quad D_{ov}\gamma_5|i\rangle = \lambda_i^*\gamma_5|i\rangle. \tag{4.10}$$

Therefore the low-mode source can be written as

$$\eta^L = \sum_i^n (|i\rangle\langle i| + \gamma_5|i\rangle\langle i|\gamma_5)|\eta\rangle. \tag{4.11}$$

Then the high-mode propagator G^H and low-mode propagator G^L are defined as

$$D(m, \rho)G^H = \eta^H, \quad D(m, \rho)G^L = \eta^L, \quad G = G^L + G^H. \tag{4.12}$$

The low-mode propagator can be easily calculated using spectral theorem and Eq. (4.9),

$$G^L = \sum_i \left[\frac{|i\rangle\langle i|\eta\rangle}{\rho\lambda_i + m\left(1 - \frac{\lambda_i}{2}\right)} + \frac{\mp\gamma_5|i\rangle\langle i|\eta\rangle}{\rho\lambda_i^* + m\left(1 - \frac{\lambda_i^*}{2}\right)}\right]. \tag{4.13}$$

Now let's go back to Eq. (4.4), and change the notation,

$$\langle P^{\pm}\chi(y)\bar{\chi}(x)\rangle = \left\langle G_{NN}\left(\bar{G}, \bar{G}, \bar{G}\right)\right\rangle, \tag{4.14}$$

in which $\bar{G}$-s are the Z_3 noise estimated quark propagator calculated from a *grid source*, and each of them has a θ_i accompanied. For simplicity, let us also drop the angular bracket,

$$G_{NN}(\bar{G}, \bar{G}, \bar{G}) = G_{NN}\left(\bar{G}^H + \bar{G}^L,\ \bar{G}^H + \bar{G}^L,\ \bar{G}^H + \bar{G}^L\right). \tag{4.15}$$

Notice that function G_{NN} is just a multiplication of all its variables with some gamma structure. Therefore it can be expanded into [8]

$$\begin{aligned} G_{NN} =& G_{NN}(\bar{G}^H, \bar{G}^H, \bar{G}^H) + G_{NN}(\bar{G}^L, \bar{G}^L, \bar{G}^L) \\ &+ G_{NN}(\bar{G}^L, \bar{G}^H, \bar{G}^H) + G_{NN}(\bar{G}^H, \bar{G}^L, \bar{G}^H) + G_{NN}(\bar{G}^H, \bar{G}^H, \bar{G}^L) \\ &+ G_{NN}(\bar{G}^H, \bar{G}^L, \bar{G}^L) + G_{NN}(\bar{G}^L, \bar{G}^H, \bar{G}^L) + G_{NN}(\bar{G}^L, \bar{G}^L, \bar{G}^H). \end{aligned} \tag{4.16}$$

For the term $G_{NN}(\bar{G}^L, \bar{G}^L, \bar{G}^L)$, since one can calculate the exact low mode propagator from the low-lying eigenvectors, it can be substituted with its exact counterpart $\sum_i G_{NN}(G_i^L, G_i^L, G_i^L)$, in which G_i^L is the exact low mode propagator calculated from the *point source* at the ith grid point. For terms like $G_{NN}(\bar{G}^L, \bar{G}^L, \bar{G}^H)$ that involve two low mode propagators, one can still substitute them with the exact propagators, but will have to multiply back the Z_3 noise in order to work with the noise-estimated high mode propagator, and therefore it becomes $\sum_i \theta_i^2 G_{NN}(G_i^L, G_i^L, \bar{G}^H)$. Thus the nucleon two-point function becomes

$$\begin{aligned} G_{NN} =& G_{NN}(\bar{G}^H, \bar{G}^H, \bar{G}^H) \\ &+ G_{NN}(\bar{G}^L, \bar{G}^H, \bar{G}^H) + G_{NN}(\bar{G}^H, \bar{G}^L, \bar{G}^H) + G_{NN}(\bar{G}^H, \bar{G}^H, \bar{G}^L) \\ &+ \sum_i \theta_i^2 \left[G_{NN}(G_i^L, G_i^L, \bar{G}^H) + G_{NN}(G_i^L, \bar{G}^H, G_i^L) + G_{NN}(\bar{G}^H, G_i^L, G_i^L) \right] \\ &+ \sum_i G_{NN}(G_i^L, G_i^L, G_i^L) \end{aligned} \tag{4.17}$$

This technique is named "low-mode substitution". By replacing noise-estimated low mode propagators with its exact version, noise/signal ratio can be improved tremendously. Figure 4.4 shows a comparison among nucleon two-point functions calculated from a point source, a grid source with Z_3 noise, and with low mode substitution. As one can see, Z_3 noises along with low-mode substitution lower the errorbar of fitted nucleon mass by roughly 3 folds.

In order to use low-mode substitution, one needs first a number of the low-lying eigen modes. These are usually calculated with the Arnoldi iteration algorithm. It is a time-consuming process; however it does not only enable one to use techniques such as low-mode substitution, but also accelerates the inversion significantly [11].

4.4 The variational method

The variational method is a powerful tool for the analysis of excited states [12]. It is now widely adopted in hadron spectroscopy studies. Suppose we have a matrix of 2-point correlation functions

$$G_{ij}(t) = \langle \chi_i(t) \bar{\chi}_j(t) \rangle = \sum_n \langle 0|\chi_i|n\rangle \langle n|\bar{\chi}_j|0\rangle e^{-E_n t},$$

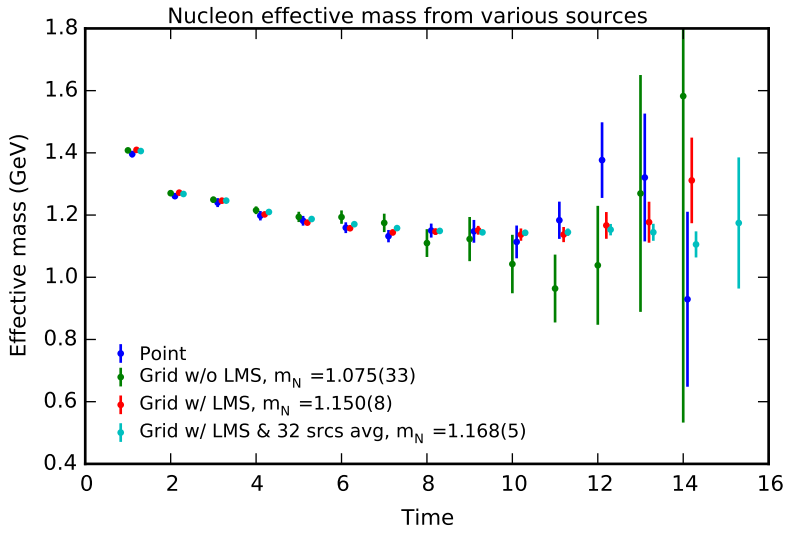

Figure 4.4: Comparison among nucleon two-point functions calculated from a point source, a grid source with Z_3 noise, and with low mode substitution. The blue points are calculated from a point smeared source; the green points are calculated from grid smeared source with Z_3 noises, but without low-mode substitution; the red and cyan points are calculated from grid smeared source with Z_3 noises and low-mode substitution. All these are calculated from 203 configuration with 2 sources for each configuration, except for the cyan points, where 32 sources per configuration, and high mode propagators are calculated with low precision.

in which i and j denote different types of operator, and zero momentum projection is taken for simplicity. In practice, the matrix usually consists of different combinations of source/sink smearing sizes, or interpolation operators. It is then proved [12] that if $\lambda_n(t)$ are the eigenvalues of $G(t)$, then

$$\lambda_n(t) = c_n e^{-E_n t}\left[1 + O(e^{-\Delta E_n t})\right], \tag{4.18}$$

in which $\Delta E_n = E_{n+1} - E_n$. However, at large t, the error on $G(t)$ becomes large, and therefore $e^{-\Delta E_n t}$ is not clearly bounded. It is more practical to look at generalized eigenvalue problem

$$G(t)v = \lambda(t, t_0)G(t_0)v,$$

in which t_0 is usually small. Since $G(t_0)v = \lambda(t_0)v$, it is obvious that $\lambda_n(t, t_0) = e^{-E_n(t-t_0)}$. This eigenvalue problem can be rewritten as

$$G(t)G(t_0)^{-\frac{1}{2}}G(t_0)^{\frac{1}{2}}v = \lambda(t, t_0)G(t_0)^{\frac{1}{2}}G(t_0)^{\frac{1}{2}}v.$$

Define $v' = G(t_0)^{\frac{1}{2}}v$, then

$$G(t_0)^{-\frac{1}{2}}G(t)G(t_0)^{-\frac{1}{2}}v' = \lambda(t, t_0)v'. \tag{4.19}$$

Therefore, in order to find the energy levels, we only need to choose an appropriate t_0, and diagonalize $G(t_0)^{-\frac{1}{2}}G(t)G(t_0)^{-\frac{1}{2}}$ on all time slices.

The variational method is a well-defined and systematic way to extract energy levels. However it does suffer from several disadvantages,

- The existence of the ΔE_n term in Eq. (4.18) means we can only acquire upper bound of energy levels.
- It is required to have at least several source/sink operator combinations. For expensive fermion actions such as the overlap fermion, this could be impractical depending on the target precision.
- As shown in chapter 6, we suspect the result may be sensitive to the choice of operators.

Chapter 5

Nucleon Momentum Fraction Carried by Quarks

5.1 Introduction

The understanding of the structure of nucleon has been one of the central issues in hadron physics. For instance, the parton distribution functions (PDFs) have been studied extensively, and the observation of scaling violation in PDFs provides the cradle for the establishment of the fundamental theory, QCD. Yet, there exist many unresolved questions on the structure of the nucleon. Ever since the EMC experiment showed that the proton spin carried by quarks is small [1], large effort has been made in both the experiments and the theoretical frontiers to identify all the contributions to the nucleon spin. Calculating the momentum fraction $\langle x \rangle$ is an integral part of the study of this subject.

However, it has been found that calculating the disconnected insertion contribution to this quantity, which is necessary for the strange momentum fraction, is very difficult. Most lattice calculations are done for the connected insertion contribution. So far, only one quenched calculation exists that includes all contributions to the nucleon spin [13], as well as one dynamical clover fermion calculation on the strange momentum fraction [14]. In this paper, we calculate the strange momentum fraction with the overlap fermion on $2+1$ flavor domain wall fermion configurations with the help of an array of lattice techniques. We also calculate the momentum fraction in the u/d channel for the disconnected insertion (DI), and take the ratio between strange and u/d channel in DI. In the end, we compare our result with previous lattice calculations, as well as current global analyses of parton distribution at small x.

5.2 Deep Inelastic Scattering

The scattering amplitude of deep inelastic scattering can be written as

$$iM = (-ie^2)\left(\frac{-ig_{\mu\nu}}{q^2}\right)\langle k'|j_l^\mu(0)|k, s_l\rangle\langle X|j_h^\nu(0)|p, \lambda\rangle, \tag{5.1}$$

in which s_l in the polarization of the initial lepton, λ is the polarization of the initial hadron, and j_l, j_h are the leptonic and hadronic electromagnetic current, respectively. The differential cross section is

$$\begin{aligned} d\sigma &= \sum_X \int \frac{d^3k'}{(2\pi)^3 2E'}(2\pi)^4\delta^4(k+p-k'-p_X)\frac{|M|^2}{(2E)(2M)} \\ &= \sum_X \int \frac{d^3k'}{(2\pi)^3 2E'}(2\pi)^4\delta^4(k+p-k'-p_X)\frac{e^4}{4Q^4EM} \\ &\quad \langle p, \lambda|j_h^\mu(0)|X\rangle\langle X|j_h^\nu(0)|p, \lambda\rangle\langle k, s_l|j_{l\mu}(0)|k'\rangle\langle k'|j_{l\nu}(0)|k, s_l\rangle \end{aligned} \tag{5.2}$$

By convention, the leptonic tensor is defined as

$$l^{\mu\nu} = \sum_{\text{final spin}} \langle k'|j_{l\nu}(0)|k, s_l\rangle\langle k, s_l|j_{l\mu}(0)|k'\rangle, \tag{5.3}$$

and the hadronic tensor is defined as

$$W^{\mu\nu}(p, q, \lambda', \lambda) = \frac{1}{4\pi}\int d^4x\, e^{iq\cdot x}\langle p, \lambda'|[j_\mu(x), j_\nu(0)]|p, \lambda\rangle. \tag{5.4}$$

Note that

$$\begin{aligned} \langle p, \lambda'|j_\mu(x)|X\rangle &= \langle p, \lambda'|j_\mu(x)|X\rangle e^{i(p-p_X)\cdot x}, \\ \langle X|j_\mu(x)|p, \lambda\rangle &= \langle X|j_\mu(x)|p, \lambda\rangle e^{i(p_X-p)\cdot x}, \end{aligned} \tag{5.5}$$

therefore

$$\begin{aligned} W_{\mu\nu} = \frac{1}{4\pi}(2\pi)^4 \sum_X \big[&\delta^4(q+p-p_X)\langle p, \lambda'|j_\mu(0)|X\rangle\langle X|j_\nu(0)|p, \lambda\rangle \\ &- \delta^4(q+p_X-p)\langle p, \lambda'|j_\nu(0)|X\rangle\langle X|j_\mu(0)|p, \lambda\rangle\big]. \end{aligned} \tag{5.6}$$

However, only the first delta function can be satisfied by the kinematics. Therefore

$$d\sigma = \frac{e^4}{Q^4}\int \frac{d^3k'}{(2\pi)^3 2E'}\frac{4\pi l_{\mu\nu}W_{\mu\nu}(p, k-k', \lambda, \lambda)}{4EM}, \tag{5.7}$$

$$\Rightarrow \frac{d^2\sigma}{dE'd\Omega} = \frac{e^4}{16\pi^2Q^4}\frac{E'}{ME}l^{\mu\nu}W_{\mu\nu}(p, q, \lambda, \lambda). \tag{5.8}$$

For spin-1/2 target, the hadronic tensor is conventionally arranged in terms of structure functions

$$\begin{aligned} W_{\mu\nu} = F_1\left(-g_{\mu\nu}+\frac{q_\mu q_\nu}{q^2}\right) + \frac{F_2}{p\cdot q}\left(p_\mu - \frac{p\cdot q q_\mu}{q^2}\right)\left(p_\nu - \frac{p\cdot q q_\nu}{q^2}\right) \\ + \frac{ig_1}{p\cdot q}\epsilon_{\mu\nu\lambda\sigma}q^\lambda s^\sigma + \frac{ig_2}{(p\cdot q)^2}\epsilon_{\mu\nu\lambda\sigma}q^\lambda(p\cdot q s^\sigma - s\cdot q p^\sigma) \end{aligned} \tag{5.9}$$

One way to evaluate the hadronic tensor Eq. (5.4) is operator product expansion (OPE). For a production of two local operator $J_a(x)$ and $J_b(0)$,

$$\lim_{x\to 0} J_a(x)J_b(0) = \sum_k c_{abk}(x)O_k(0), \tag{5.10}$$

where O_k is a local operator. For QCD, the operators in the expansion are quark and gluon operators $O_{dn}^{\mu_1\cdots\mu_n}$ with arbitrary spin n and dimension d. The leading term in the expansion has twist $t = d-n = 2$. Note that O is independent of the direction of momentum q^μ; only the proton momentum P^μ is available to carry the vector indices. Therefore the spin-averaged matrix element of O can be written as

$$\langle P|O_{dn}^{(f)\mu_1\cdots\mu_n}|P\rangle = 2A_f^n P^{\mu_1}\cdots P^{\mu_n} - \text{traces}, \tag{5.11}$$

in which f labels quark flavor. For twist-2, the simplest operators are

$$\langle P|\bar\psi_f\gamma^\mu\psi_f|P\rangle = 2P^\mu A_f^1, \tag{5.12}$$

in which A_f^1 is the number of quarks minus antiquarks of flavor f in state $|P\rangle$, and

$$\langle P|\bar\psi_f\gamma^{\{\mu}iD^{\nu\}}\psi_f|P\rangle = 2P^\mu P^\nu A_f^2, \tag{5.13}$$

in which $\gamma^{\{\mu}iD^{\nu\}} = \gamma^\mu iD^\nu - \gamma^\nu iD^\mu$, and the operator is the QCD energy-momentum tensor. Therefore A_f^2 is the fraction of the total energy-momentum of the proton that is carried by the quark flavor f.

5.3 Formalism

X. Ji has proposed that in Minkowski space, the nucleon matrix element of energy-momentum tensor can be split into form factors as [15]

$$\langle P'|T^{\mu\nu}|P\rangle = \bar u(P')\left[A(Q^2)\gamma^{\{\mu}\bar P^{\nu\}} + \frac{B(Q^2)}{2m}\bar P^{\{\mu}i\sigma^{\nu\}\alpha}Q_\alpha + \frac{C(Q^2)}{m}(Q^\mu Q^\nu - g^{\mu\nu}Q^2) + \bar C(Q^2)g^{\mu\nu}m\right]u(P), \tag{5.14}$$

in which $\bar P = (P+P')/2$, $Q = P'-P$. For forward case, $P = P'$, coefficient $A(0)$ gives the momentum fraction of the nucleon carried by quarks, i.e. $A(0) = \langle x\rangle$. For $\mu = 0$, $\nu = i$ specifically,

$$\langle P|T^{\mu\nu}|P\rangle = \langle P|\bar\psi\gamma^{\{0}(iD)^{i\}}\psi|P\rangle = \frac{A(0)}{2}\bar u(P)(P^0\gamma^i + P^i\gamma^0)u(P). \tag{5.15}$$

Using the Gordon identity

$$\bar u(P')\gamma^\mu u(P) = \bar u(P')\left(\frac{\bar P^\mu}{m} + \frac{i\sigma^{\mu\nu}Q_\nu}{2m}\right)u(P),$$

$$\Rightarrow \bar u(P)\gamma^\mu u(P) = \bar u(P)\frac{P^\mu}{M}u(P), \tag{5.16}$$

it follows that

$$\langle P|\bar{\psi}\gamma^{\{0}(iD)^{i\}}\psi|P\rangle = \frac{A(0)}{m}p^0p^i = \frac{A(0)}{m}Ep^i.$$

In euclidean space, this becomes

$$\langle P|\bar{\psi}\gamma^{\{4}(iD)^{i\}}\psi|P\rangle = \frac{A(0)}{m}Ep_i.$$

On the lattice, this becomes

$$\langle P|\bar{\psi}\gamma^{\{4}(iD)^{i\}}\psi|P\rangle = \frac{p_i}{N}A(0) \tag{5.17}$$

In order to calculate the strange contribution to nucleon $\langle x\rangle$, we must insert the twist-2 operator into a quark loop. Therefore we need to calculate the disconnected insertion of a three-point correlation function on the lattice.

Continue from Eq. (3.28), and use Eq. (5.17)

$$\mathrm{Tr}(P_+G_{NON}(t_2,p)) \to a^6e^{-E_0(t_2-t_0)}\langle x\rangle p_i\,|\lambda|^2\frac{m}{E}\left(1+\frac{E}{m}\right). \tag{5.18}$$

Recall from Eq. (3.12) that at large time, the nucleon two-point function is

$$\mathrm{Tr}(P_+G_{NN}(t,p)) \to a^6e^{-E_0(t-t_0)}|\lambda|^2\frac{m}{E}\left(1+\frac{E}{m}\right). \tag{5.19}$$

Therefore, if we calculate the following ratio between the three-point function and the two-point function, we can extract $\langle x\rangle$,

$$\frac{1}{p_i}\frac{\mathrm{Tr}[P_+G_{NON}(t_2,p_i)]}{\mathrm{Tr}[P_+G_{NN}(t_2,p_i)]} \to \langle x\rangle. \tag{5.20}$$

However, the expression above is not enough if we want to calculate it on the lattice. On the lattice, quark propagators are the smallest element one can compute. We need to express the three-point function in terms of quark propagators. Recall that our operator O_{4i} is from

$$\bar{O}_{4i}(x) = -\frac{i}{2}\left[\bar{\psi}(x)\gamma_4\overrightarrow{D}_i\psi(x) - \bar{\psi}(x)\gamma_4\overleftarrow{D}_i\psi(x)\right], \tag{5.21}$$

$$O_{4i} = \frac{1}{2}(\bar{O}_{4i} + \bar{O}_{i4}). \tag{5.22}$$

And covariant derivatives are replaces with differences between neighbors,

$$\begin{aligned}\bar{O}_{4i}(x) = -\frac{i}{4a}\Big[&\bar{\psi}(x)\gamma_4U_i(x)\psi(x+\hat{i}) - \bar{\psi}(x)\gamma_4U_i^\dagger(x-\bar{i})\psi(x-\hat{i})\\ &+\bar{\psi}(x-\hat{i})\gamma_4U_i(x-\hat{i})\psi(x) - \bar{\psi}(x+\hat{i})\gamma_4U_i^\dagger(x)\psi(x)\Big].\end{aligned} \tag{5.23}$$

Therefore

$$\begin{aligned}
&\langle \chi(x_2) O(x_1) \bar{\chi}(x_0) \rangle \\
= &-\frac{i}{4a} \int \mathcal{D}u \mathcal{D}\bar{u} \mathcal{D}d \mathcal{D}\bar{d} \mathcal{D}\psi \mathcal{D}\bar{\psi} \, (u^T(x_2) C\gamma_5 d(x_2)) u(x_2) \\
&\Big[\bar{\psi}(x_1)\gamma_4 U_i(x_1)\psi(x_1+\hat{i}) - \bar{\psi}(x_1)\gamma_4 U_i^\dagger(x_1-\bar{i})\psi(x_1-\hat{i}) \\
&+ \bar{\psi}(x_1-\hat{i})\gamma_4 U_i(x_1-\hat{i})\psi(x_1) - \bar{\psi}(x_1+\hat{i})\gamma_4 U_i^\dagger(x_1)\psi(x_1) \Big] \\
&(\bar{d}(x_0) C\gamma_5 \bar{u}^T(x_0))\bar{u}(x_0),
\end{aligned} \tag{5.24}$$

in which color indices are understood and ignored. Note that ψ can be any flavor (when it is u/d, the integration measure is just $\mathcal{D}u\mathcal{D}\bar{u}\mathcal{D}d\mathcal{D}\bar{d}$). However if ψ is a heavy flavor, then the ψ field can only contract to itself, and the u and d part of the expression contracts to a normal nucleon propagator, as shown in Eq. (3.31). Specifically,

$$\mathrm{Tr}[P_+ G_{NON}(t_2, \vec{p})] = \langle C_2(t_2, \vec{p}) C_O(t_1) \rangle, \quad C_O(t) = \sum_{\vec{x}} \frac{1}{2}(C_{4i}(x) + C_{i4}(x)) \tag{5.25}$$

in which C_2 is the nucleon propagator in each configuration, and

$$\begin{aligned}
C_{4i}(x) = -\frac{i}{4a}\big(&\mathrm{Tr}[G(x+\hat{i}, x)\gamma_4 U_i(x)] - \mathrm{Tr}[G(x-\hat{i}, x)\gamma_4 U_i^\dagger(x-\hat{i})] \\
&+ \mathrm{Tr}[G(x, x-\hat{i})\gamma_4 U_i(x-\hat{i})] - \mathrm{Tr}[G(x, x+\hat{i})\gamma_4 U_i^\dagger(x)]\big).
\end{aligned} \tag{5.26}$$

As shown in this expression, the operator part of the calculation is computed by generating propagators that comes from a point and ends up at its neighbors, and multiply it by the correct gauge link and gamma matrices. This quantity is usually called the "loop". Therefore

$$\frac{1}{|\vec{p}|}\frac{\mathrm{Tr}[P_+ G_{NON}(t_2, p)]}{\mathrm{Tr}[P_+ G_{NN}(t_2, p)]} = \frac{1}{|\vec{p}|}\frac{\langle C_2(t_2, \vec{p}) C_O(t_1) \rangle}{\langle C_2(t_2, \vec{p}) \rangle} \to \langle x \rangle. \tag{5.27}$$

In reality, this is done by calculating parity projected nucleon two-point function, and the loop, and then take an appropriate ratio.

5.4 Calculation details

Our calculation uses the $2+1$-flavor domain wall fermion configurations generated by the RBC/UKQCD collaboration [16, 17]. A wide range of quark masses are involved in this study spanning from physical pion mass to strange mass. The three lattices involved are listed in Table 5.1.

The nucleon 2-point function is calculated with low-mode substitution described in section 4.3. Grid sources arranged in 2-2-2 (or 4-4-4 for the 48I lattice) geometry with Z_3 noises are used, meaning two grid points are placed in each spatial direction. In order to

Table 5.1: The parameters for the RBC/UKQCD configurations.

Lattice	Size	a (fm)	m_s^{sea} (MeV)	m_π (MeV)	# confs
24I	$24^3 \times 64$	0.1105(3)	120	330	203
32I	$32^3 \times 64$	0.0828(3)	110	300	309
48I	$48^3 \times 96$	0.1141(3)	94.9	139	81

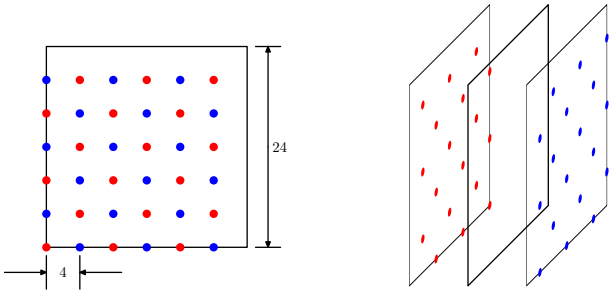

Figure 5.1: Source scheme for the loop, on the 24I lattice. The right figure shows the grid points on different time slices in each diluted inversion.

further boost the signal/noise ratio, 32 sources are inverted for each configuration, shifted in space and time. Low precision calculation is used in the high mode part in order to increase computation speed.

Similarly, the loop is calculated with a 6-6-6 grid source with Z_4 noises, placed at every other time slices in a even-odd fashion. The high mode part is also calculated with low precision. Like for the 2-point function, 32 sources are inverted for each configuration, shifted in space and time. An illustration of the sources used in the loop calculation is shown in Figure 5.1.

With Eq. (5.20), nucleon two-point function projected to finite momentum is required. If we use a point source, momentum can be any integer. However for the grid source we use, only a subset of momenta can be acquired. Specifically, for a 2-2-2 configuration, we can only project the correlation function to zero momentum and momenta 2, 4, etc. (in lattice unit). In order to acquire momentum 1, an extra set of grid sources needs to be inverted. These grid sources are multiplied by a phase factor $e^{ip_x x} + e^{ip_y y} + e^{ip_z z}$ before inversion, and produce momenta 1, 3, etc. And thus we recover a complete set of momenta.

The three-point/two-point function ratio is then fitted to acquire the value of $\langle x \rangle$. To address the effect of excited states, we go beyond Eq. (5.20), and take into account the first excited state. Take Eq. (3.21), the next leading term is $n_1 = 0$, $n_2 = 1$, or $n_1 = 1$, $n_2 = 0$. Define

$$M_{ij} = \langle 0|\chi|N_i\rangle\langle N_i|O|N_j\rangle\langle N_j|\bar{\chi}|0\rangle,$$

where N_i is the ith nucleon state (N_0 being the ground state). Then

$$G_{NON}(t_2, t_1) = e^{-E_0 t_2}[M_{00} + e^{-\Delta(t_2-t_1)}M_{10} + e^{-\Delta t_1}M_{01} + O(e^{-\Delta' t_1})],$$

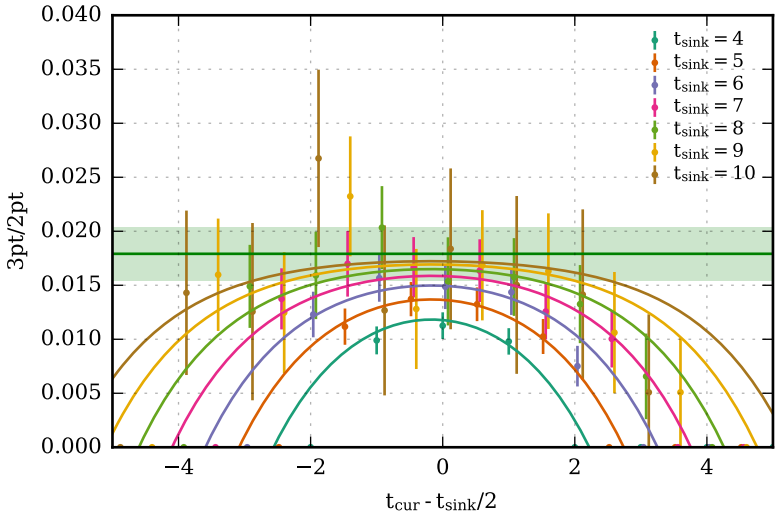

Figure 5.2: 3-point/2-point function ratio from the 24I lattice, the 2-point function is with pion mass $\sim 340\,\mathrm{MeV}$, while the loop is with pion mass $\sim 640\,\mathrm{MeV}$. The green transparent bar shows the fitted plateau (C_0 in Eq. (5.28)). Note that the plot is shifted in time by $t_1 - t_2/2$, so for all the sink times, the plateaus are centered at 0.

in which the source time is set to zero, $\Delta = E_1 - E_0$, and $\Delta' = E_2 - E_0$. For the 2-point functions, we only write the leading term,

$$G_{NN}(t_2) = e^{-E_0 t_2}\left[\langle 0|\chi|N_0\rangle\langle N_0|\bar{\chi}|0\rangle + O(e^{-\Delta t_2})\right].$$

Therefore the 3-point/2-point ratio is in the form of

$$\frac{1}{|\vec{p}|}\frac{G_{NON}(t_2,t_1)}{G_{NN}(t_2)} = C_0 + C_1 e^{-\Delta(t_2-t_1)} + C_2 e^{-\Delta t_1}. \tag{5.28}$$

If we take the constant term C_0, we should recover the approximation Eq. (5.27), and acquire the appropriate value of $\langle x\rangle$. It is well-known that for this kind of 3-point/2-point ratio, the summed method [18] helps isolating the ground state in the presence of excited states, by summing over the insertion time t_1,

$$\frac{1}{|\vec{p}|}\sum_{t_1=0}^{t_2-1}\frac{G_{NON}(t_2,t_1)}{G_{NN}(t_2)} = C_0 t_2 + \frac{e^{-\Delta} - e^{-\Delta(t_2+1)}}{1-e^{-\Delta}}C_1 + \frac{1-e^{-\Delta t_2}}{1-e^{-\Delta}}C_2. \tag{5.29}$$

Note that the values of C_0, C_1, C_2, and Δ are shared between Eq. (5.28) and Eq. (5.29), and are used as parameters when we fit these two models simultaneously with the 3-point/2-point ratio data.

Table 5.2: Renormalization factors used in this study.

Lattice	Z_{qq}	Z_{qg}
24I	0.991	0.017
32I	1.026	0.0096
48I	0.986	0.018

Table 5.3: The fitted parameters, with $\chi^2/\text{DoF} = 0.2$

	c1	c2	c3	c4	c5	c7	c8	c9	c10	c11	c12	c13
Value	0.053	0.16	0.025	0.063	0.12	0.014	−0.044	−0.0024	−0.73	−0.76	0.76	0.93
Error	0.02	0.097	0.028	0.021	0.09	0.03	0.1	0.12	0.36	0.37	0.75	0.79

5.5 Results

We calculate 2-point/3-point function ratios from all quark mass combinations. An example of such ratio is shown in Figure 5.2. These ratios are renormalized and matched to $\overline{\text{MS}}$ scheme at 2 GeV, with consideration of glue mixing.

$$\langle x\rangle_q = Z_{qq}\langle x\rangle_q^{\text{bare}} + Z_{qg}\langle x\rangle_g, \tag{5.30}$$

in which $\langle x\rangle_g = 0.4$ is the glue momentum fraction in nucleon, acquired from the CTEQ global analysis [19, 20]. The renormalization factors Z_{qq} and Z_{gq} are calculated from lattice perturbation theory under 1-loop order, and have the values shown in Table 5.2.

We then extrapolate $\langle x\rangle_{u/d}^{\text{DI}}$ and $\langle x\rangle_s$ simultaneously to physical pion mass, large volume, and continuum limit with the following functional form [21]

$$\begin{aligned}\langle x\rangle_s &= c_1 + c_2 m_{\pi,vv}^2 + c_{10} m_{\pi,vs}^2 + c_{12} m_{\pi,vs}^3 + c_3 a^2 + c_8 \exp(-m_{\pi,vv} l)\\ \langle x\rangle_{u/d}^{\text{DI}} &= c_4 + c_5 m_{\pi,vv}^2 + c_{11} m_{\pi,vs}^2 + c_{13} m_{\pi,vs}^3 + c_7 a^2 + c_9 \exp(-m_{\pi,vv} l),\end{aligned} \tag{5.31}$$

in which $m_{\pi,vv}$ is the valence-valence pion mass, and the c's are fitting parameters. The valence-sea quark mass is defined as

$$m_{\pi,vs}^2 = \frac{1}{2}(m_{\pi,vv}^2 + m_{\pi,ss}^2) + a^2\Delta_{\text{mix}},$$

where $m_{\pi,ss}$ is the sea-sea pion mass. The effect of Δ_{mix} is a small shift ($10 \sim 30$ MeV) on the pion mass due to the mismatch between the sea and valence QCD action [22]. The fitting is done with 1000 bootstrap samples for each ensemble. Value of χ^2 for this fit is 0.2, and the value of the parameters are listed in Table 5.3. The extrapolated values at physical pion mass and continuum are

$$\langle x\rangle_s = 0.046(15), \quad \langle x\rangle_{u/d}^{\text{DI}} = 0.055(16). \tag{5.32}$$

We also plot the fitting result in Figure 5.3 and Figure 5.4. Lattice spacing dependence is found to be negligible in our study.

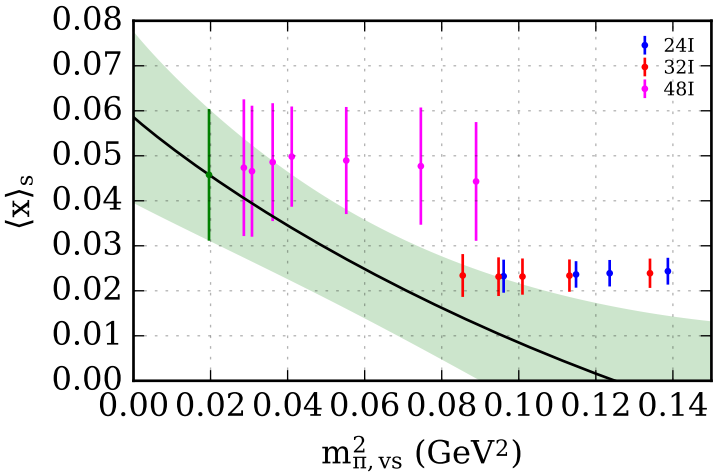

Figure 5.3: Chiral and continuum extrapolation of $\langle x \rangle_s$. The renormalized three-point function slopes from the 24I, 32I, and 48I lattice are denoted by blue, red, and magenta bars, respectively. The black curve shows the chiral fit line at continuum. The green bar shows the extrapolated value.

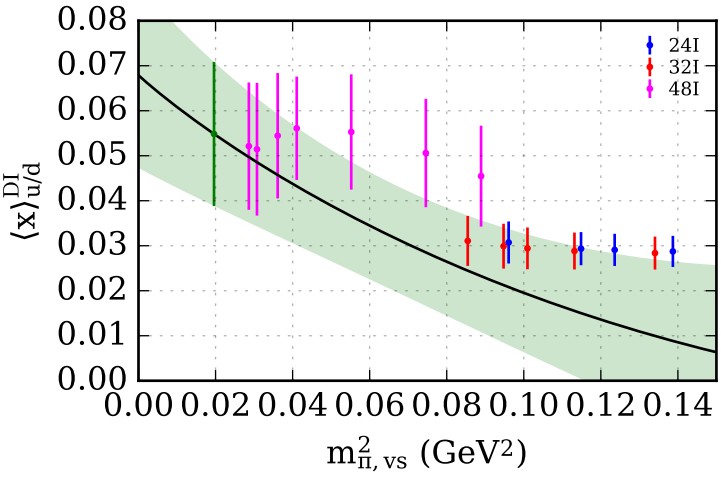

Figure 5.4: Chiral and continuum extrapolation of $\langle x \rangle^{DI}_{u/d}$. The renormalized three-point function slopes from the 24I, 32I, and 48I lattice are denoted by blue, red, and magenta bars, respectively. The black curve shows the chiral fit line at continuum. The green bar shows the extrapolated value.

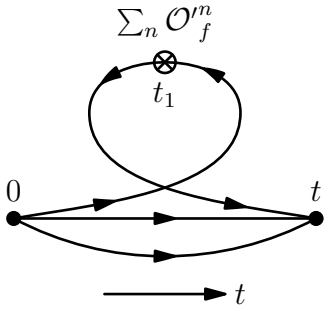

(a) Quark line diagram of the connected sea

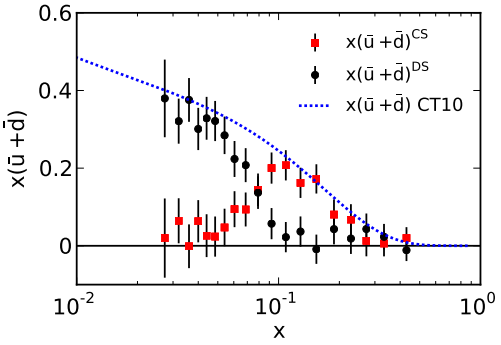

(b) Behavior of disconnected sea and connected sea as functions of x. The blue dashed line shows the distribution from CT10 [27].

Figure 5.5

Last but not least, we calculate the ratio $\langle x\rangle_s/\langle x\rangle^{DI}_{u/d}$ at physical pion mass and continuum

$$\frac{\langle x\rangle_s}{\langle x\rangle^{DI}_{u/d}} = 0.83(7). \tag{5.33}$$

It is worthwhile to compare this ratio with the global analysis shown in Figure 5.6 [23]. But before doing this, we recall that the experimental result for $\bar{u}$ and $\bar{d}$ does not exactly correspond to our lattice result of disconnected insertion; rather, part of them are from the so called "connected sea" contribution, which is the result of the diagrams shown in Figure 5.5a [24, 25]. However, the connected sea contribution behaves as $x^{-1/2}$ in the small x region, while the disconnected sea, which corresponds to the disconnected insertion on the lattice, behave as x^{-1}. Therefore at small x, only the latter survives. This is demonstrated in Figure 5.5b, in which the disconnected-sea contribution $\bar{u}^{ds}(x)+\bar{d}^{ds}(x)$ is assumed to be $(s(x)+\bar{s}(x))/R$, where R is the ratio obtained in a previous lattice result by T. Doi et al. [14], and $s(x)+\bar{s}(x)$ is taken from the HERMES result [26]. The connected sea contribution $\bar{u}^{cs}(x)+\bar{d}^{cs}(x)$ can be obtained by taking the CT10 global fit [27] and subtract out the disconnected sea part, i.e.

$$\bar{u}^{cs}(x)+\bar{d}^{cs}(x) = \bar{u}(x)+\bar{d}(x)-\frac{1}{R}(s(x)+\bar{s}(x)).$$

As shown in the plot, connected sea contribution indeed vanishes at small x. Furthermore, Figure 5.6 shows a flat behavior at small x region, therefore can be treated as a constant, and be directly compared with our lattice result Eq. (5.33). In this region, our result is compatible with the global analysis, and be used as input for future analysis.

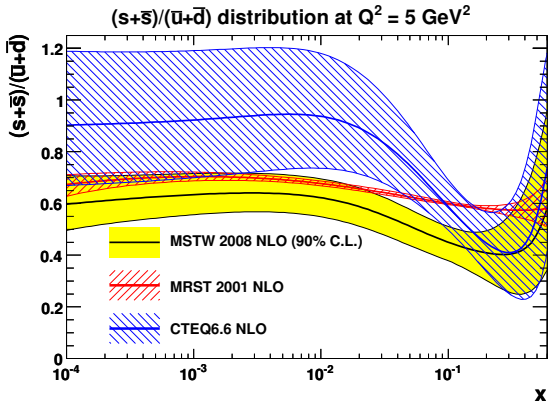

Figure 5.6: Ratio of $s + \bar{s}$ over $\bar{u} + \bar{d}$ versus x at $Q^2 = 5\,\mathrm{GeV}^2$ from various recent PDFs.

5.6 Conclusion and Discussion

In conclusion, we have studied the momentum fraction carried by quarks in nucleon with overlap fermions on $2+1$ flavors domain wall dynamical fermion configurations. We utilize an array of lattice techniques including low mode substitution and low mode averaging, as well as grid sources with Z_3 and Z_4 noises to greatly improve the signal of both the nucleon propagator and the quark loop. We find signals for $\langle x \rangle_s$ and $\langle x \rangle^{DI}_{u/d}$ with about 3.5 sigma at the physical point. After taking the ratio $\langle x \rangle_s / \langle x \rangle^{DI}_{u/d}$, we found it to be consistent with global analysis result, but with much smaller error. Since we calculate from first principle, our result can be used to further constrain the global analysis of this ratio at small x. We would also like to point out that our result is in agreement with previous lattice calculations by T. Doi et al. [14] and M. Deka et al. [13]. Note that result is obtained from a complete study at the physical pion mass, large volume and continuum limit, while the two previous result are only at the physical pion mass.

Chapter 6

The Roper Puzzle

6.1 Introduction

The nature of the lowest nucleon excited state, Roper, has been an intriguing subject since its discovery. Measured with a mass at 1430 MeV and a width of 350 MeV, it is unusual to have a radial excitation to have lower mass than the P-wave excitation ($S_{11}(1530)$). Many speculations have circulated around the nature of Roper. For example, shortly after the discovery of Roper, it has been discussed that it could be a candidate of the so-called hermaphrodite hadrons [28]. The quark model based on $SU(6)$ symmetry with color-spin interaction fails to explain this pattern of parity reversal [29]. Realistic potential calculations with linear and Coulomb potentials [30] and the relativistic quark model [31] all predict the Roper to be about 100 to 200 MeV above the experimental value with the negative parity state lying lower. The skyrmion model initially predicts a Roper mass at about 200 MeV lower than the experimental value [32, 33], and was later improved by adding a sixth order term [34]. Also with the discovery of more and more exotic hadrons, the possibility of Roper being a pentaquark state has been mentioned [35]. However, quenched calculations on the lattice with overlap fermion has indicated that at low pion mass, consistency with experiments can be achieved with three-quark interpolation field in the even parity channel [36]; it is only at higher pion mass region, that the mass of Roper becomes higher than the P-wave excitation. As shown in Figure 6.1a, this result is in contrast with other lattice results obtained from Wilson-type fermions, which are all much higher (~ 2.2 GeV) than the experimental value [37]. Similar results are obtained from dynamical fermions. As shown in Figure 6.1b, for the first excited state, the overlap result ("χQCD", magenta points) [38] is consistent with experiment value when extrapolated to physical pion mass, and is significantly lower than most results from other groups in the whole pion mass region, while the ground state masses are consistent among all groups. [39, 38, 40, 41]. In both the quenched and dynamical cases, the mass of the excited state from overlap fermion are consistently ~ 500 MeV higher than the ground state across the whole pion mass region.

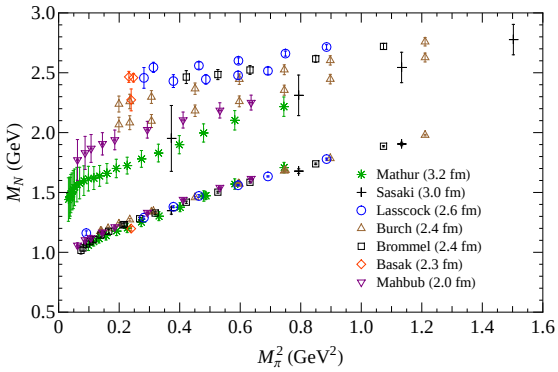

(a) Quenched results of mass of nucleon ground state and first excited state across the pion mass region. The green stars are results obtained from the overlap fermion.

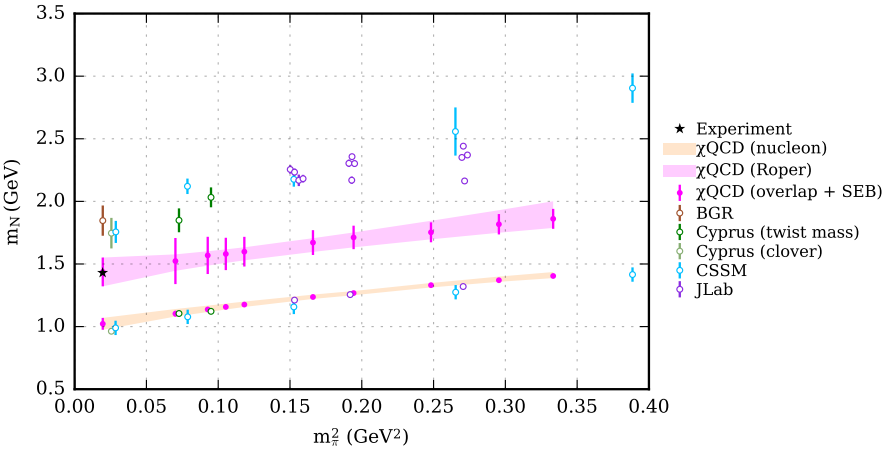

(b) Dynamical results of the mass of the nucleon ground state and excited states across the pion mass region. The light blue and purple points/band are results obtained from the overlap fermion.

Figure 6.1: Mass of the ground state and the excited states in the nucleon channel, calculated by various groups.

It is tempting to identify the significant discrepency between the overlap results and calculations from other groups as a result of distinct choices of fermion action; however, this obvious identification is also a hasty one. The overlap results are based on the Sequential Empirical Bayesian (SEB) method [42], with coulomb wall sources, while other results from Wilson-like actions are calculated with the variational approach (see section 4.4). But how much does the choice of the analysis method contribute to the discrepency? To answer this question, we isolate the dynamical result from Jefferson Lab [39], at $m_\pi = 396\,\mathrm{MeV}$, and take a lattice with identical action, quark mass, lattice spacing, and pion mass, but with a larger volume ($24^3 \times 128$ instead of $16^3 \times 128$), and perform the same calculation we did with the overlap fermion, i.e. we use a coulomb wall source and analyze the result with the SEB method. We plot the results in Figure 6.2 as the blue points.

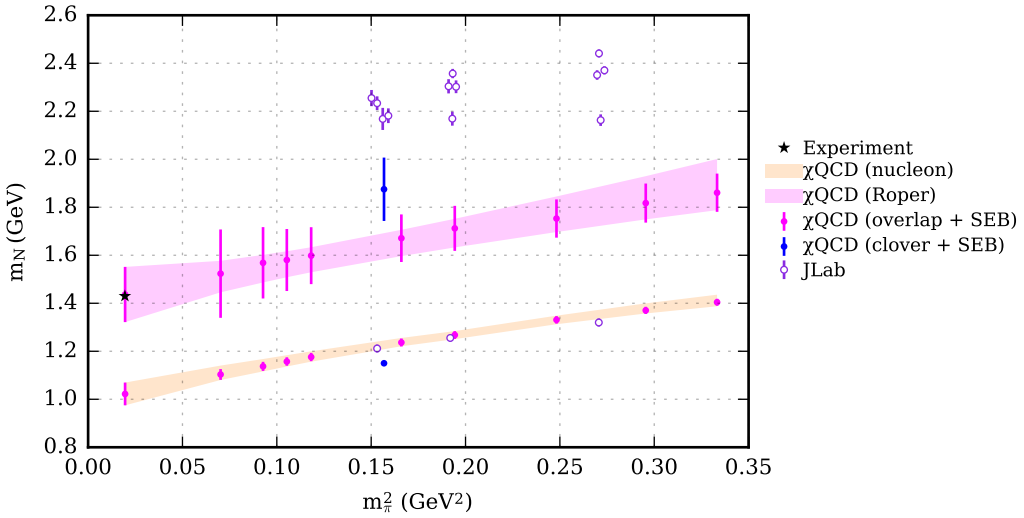

Figure 6.2: Results obtained from the anisotropic clover lattice with the SEB method, compared with that from the variational method, and from the overlap fermion with the SEB method.

As shown in the plot, the result is significantly lowered from the variational calculation by $\sim 300\,\mathrm{MeV}$, but is still higher than the overlap calculation by $\sim 250\,\mathrm{MeV}$. The latter is supposedly due to the difference in fermion action. To investigate the possible contributions to the former difference, let us turn our attention to the Roper wave function.

As reported by multiple groups [43, 44], the Roper wave function has a node at $\sim 0.8\,\mathrm{fm}$ radius as shown in Figure 6.3. And also recall that with the variational method, smeared sources/sinks with multiple smear sizes are used to construct the variational matrix. It is then vital to have an appropriate set of sources/sinks, to have reasonable overlap with the Roper state. Given that the only difference between the Roper and nucleon wave function is the node, it is natural to require that at least some of the smear sizes should be large enough to cover this important feature. If the smear size is not large enough, it may be more likely to couple to the 3S state of nucleon, whose first node is at smaller radius than Roper, and therefore results in a higher mass in variational method.

To illustrate this statement, we apply the so-called Ground State Elimination (GSE) method. Specifically, we recall that the lattice 2-point correlation functions are sum of exponentials,

$$G_{NN}(t) = \sum_n c_n e^{-E_n t} = c_0 e^{-E_0 t} + c_1 e^{-E_1 t} + \cdots$$

If we calculate two correlation functions from different operators, we acquire $G_a(t)$ and $G_b(t)$ with different set of coefficients c_0^a, c_1^a, ...and c_0^b, c_1^b, ...Then there must exist a number A, such that

$$AG_a(t) + G_b(t) = (Ac_1^a + c_1^b)e^{-E_1 t} + (Ac_2^a + c_2^b)e^{-E_2 t} + \cdots, \tag{6.1}$$

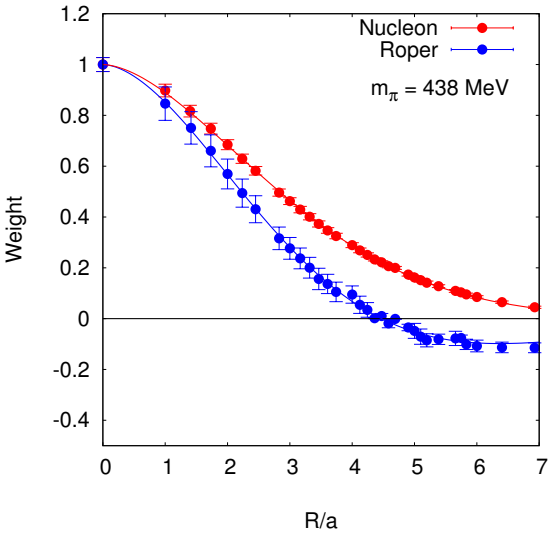

(a) The Roper wave function obtained from the overlap fermion (quenched) [43]. Lattice spacing is about 0.2 fm. Pion mass is 438 MeV

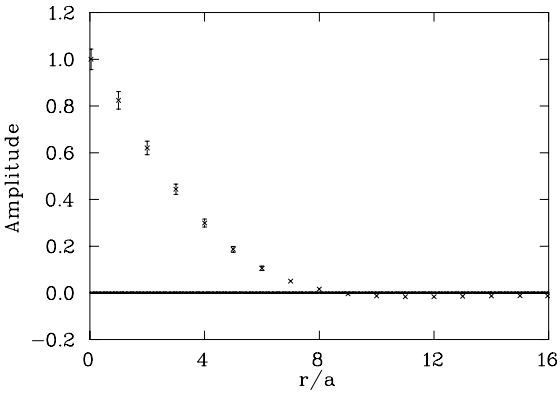

(b) The Roper wave function obtained from the improved Wilson fermion (dynamical) [44]. Lattice spacing is about 0.09 fm. Pion mass is 156 MeV

Figure 6.3: The Roper wave function, obtained by various groups.

i.e. the ground state vanishes with $Ac_0^a + c_0^b = 0$. With this we can treat the first excited state as the new ground state, and fit for its energy.

Utilizing this method, we arrive at Figure 6.4. In these figures, we compare the first excited state obtained with the GSE method, but from operator with different size. In Figure 6.4a, the result is obtained from two large sources, which have RMS radius approximately 0.63 fm and 0.86 fm. These sources are large enough to cover the node in Roper's radial wave function (note that these gaussian sources have a long tail at large distance), and therefore the mass of first excited state as acquired with the GSE method is at 1.736(28) GeV, which is compatible with what we extracted with the SEB method on the same lattice. However, if we choose a point source and small source with RMS radius of $\sim$ 0.4 fm, as shown in Figure 6.4b, the mass of the first excited state raised to about 2 GeV, which is in the range of most variation results. This result reinforces our statement that one may need to have at least a number of large sources in order to achieve a lower first excited state mass with the variational method.

6.2 Result and Discussion

Equipped with this knowledge, a natural next step is to choose a set of operators including a number of large smear sizes, and construct a variational matrix. We use the same anisotropic clover lattice as used in the SEB study, with the smearing parameters shown in Table 6.1.

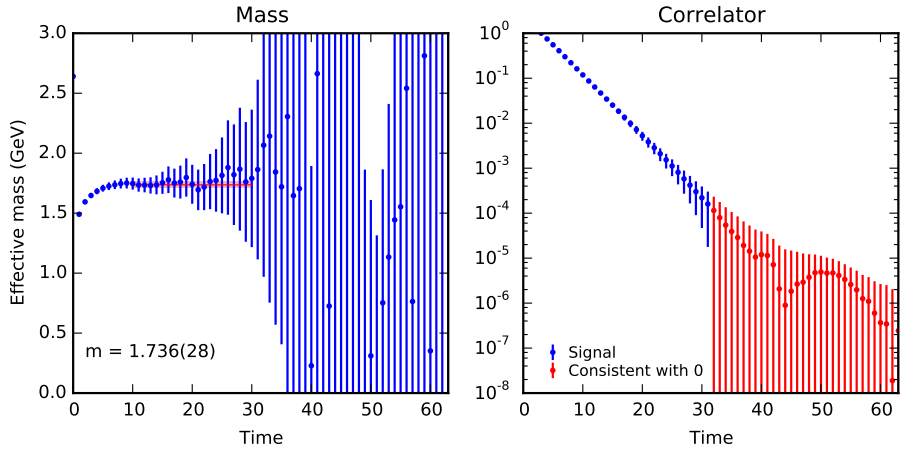

(a) Result obtained from smeared sources with $w = 7$ and $w = 11$. The mass is fitted to be $1.736(28)$ GeV, which is compatible with the blue point in Figure 6.2.

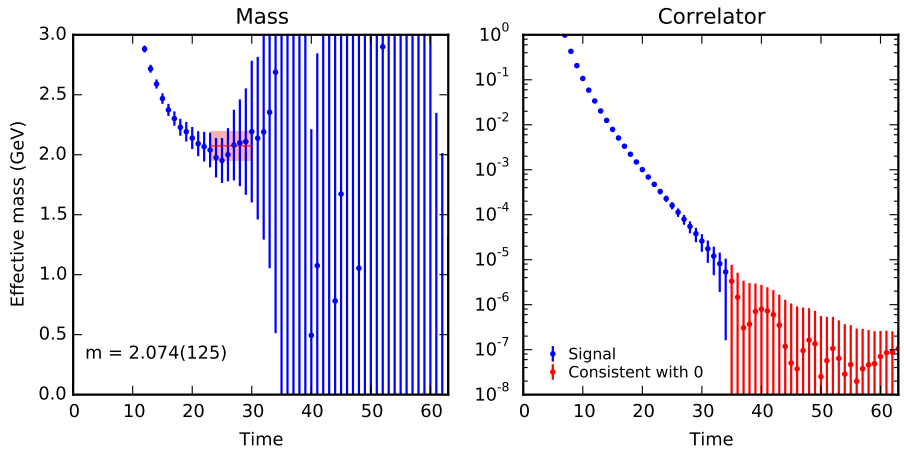

(b) Result obtained from a point source and a smeared source with $w = 4$. The mass is fitted to be $2.07(13)$ GeV, which is significantly higher than that in (a).

Figure 6.4: Correlation functions acquired with the GSE method. The $24^3 \times 128$ anisotropic clover lattice with $m_\pi = 396$ MeV is used. Effective mass is plotted on the left, and correlation function on the right. The red points in the correlation function denote the portion of data that is canceled.

Table 6.1: The smearing parameters used for our variation study.

w	Iterations	RMS radius (fm)
0 (point)	0	-
2	50	0.185
4	100	0.39
7	200	0.63
11	400	0.86

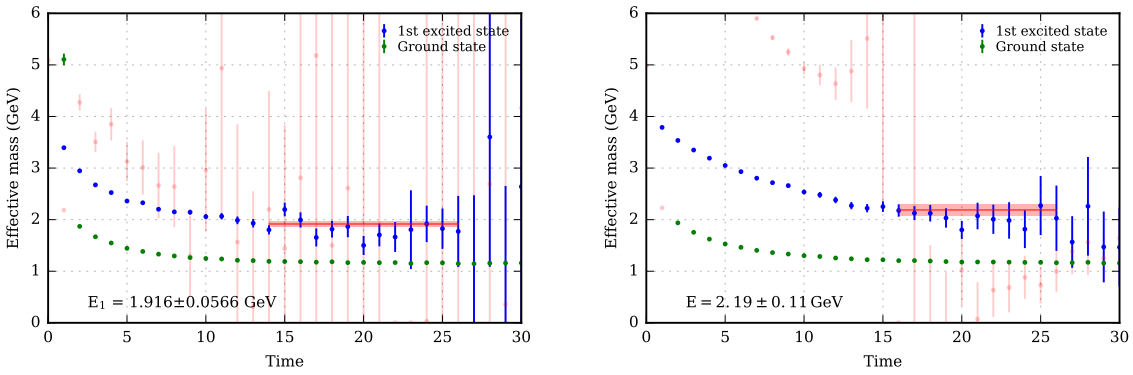

(a) Result from smear size 0, 4, 7, and 11.

(b) Result from smear size 0, 2, and 4.

Figure 6.5: Effective mass of the states extracted from the variation study. Some states are painted faintly for clarity. The red horizontal line and band shows the fit on Roper mass. Fitting result for the ground state is not drawn.

We inverted 761 configurations, on each of which we choose 36 time slices to place the source, resulting in 27396 measurements in total. Spatially the sources are randomly placed.

Result of this calculation is plotted in Figure 6.5. Interestingly, the Roper mass obtained from small operators and large operators are significantly different, at $2.19(11)$ GeV and $1.92(6)$ GeV. More importantly, the former result is compatible with the JLab result, while the latter with our result obtained with the SEB method. This confirms our statement that in order to acquire a lower Roper mass, large operators should be used to cover the node in Roper's radial wave function. However, we should also point out that the clover lattice used by JLab differs with the one we use in volume, whose effect is unknown at this point.

However, this does not explain the discrepancy between the result from overlap fermion with SEB and CSSM result near the physical point. It is argued that the low Roper mass could be due to meson-baryon interaction. This is motivated in the framework of the so-called JLMS model [45], which models effective vertices such as meson-baryon-N^*. It is found that a bare state at 1736 MeV in the P_{11} channel evolves into a pole at 1364 MeV and another at 1820 MeV, corresponding to Roper and $N^*(1710)$, respectively, due to meson-baryon interaction [46]. It is possible that the strength of these meson cloud effects differs between overlap and clover fermion, and may be an a^2 effect.

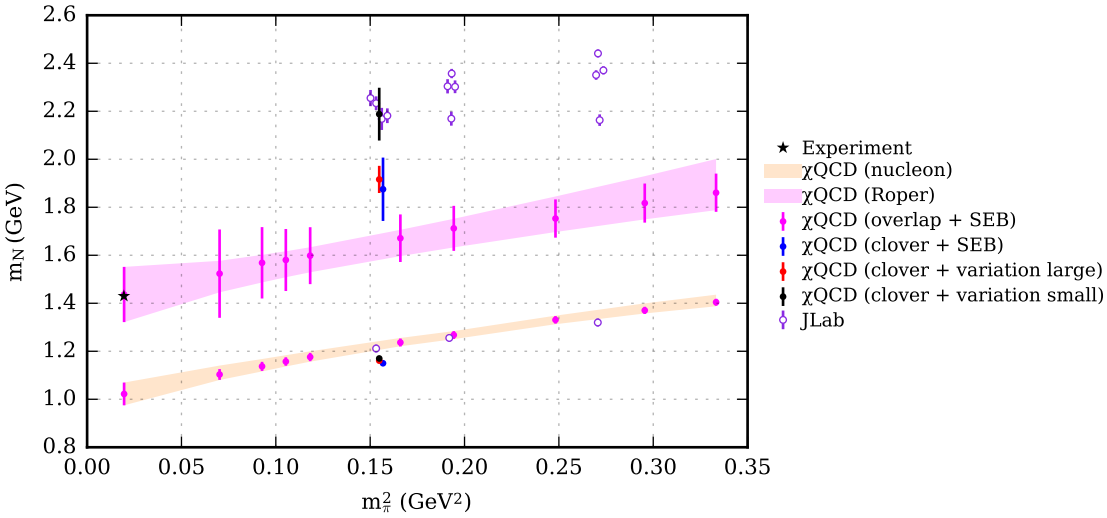

Figure 6.6: Result compared to other studies.

More importantly, it can be argued that the mass of Roper is sensitive to chiral symmetry. It is shown that in the framework of $SU(6)$ relativistic quark model, the Roper is heavier than the lightest state in the parity-odd channel. In order to achieve parity reversal, the hyperfine interaction should be flavor-dependent, and the best candidate for such an interaction is a Goldstone-boson exchange, as a result of spontaneous chiral symmetry breaking [47, 36]. It is very much likely that the Roper mass calculated with the overlap fermion is much lower than other results, because the overlap fermion satisfies the Ginsparg-Wilson relation at finite lattice spacing, while Wilson-type fermion actions only restore chiral symmetry at $a \to 0$. It is not unusual that we observe different behavior of this kind between chiral fermions and non-chiral fermions. In the quenched era, ghost states were seen in scalar two-point functions, which were results of the so-called "quenched chiral loops" [48]. Its effect is most pronounced with chiral fermions such as the overlap fermion. For example, with the overlap fermion, $\eta'\pi$ and $\eta' N$ ghost states have been reported on lattices with spacing as large as 0.2 fm [36, 49], while they can only be seen on much finer ($a < 0.06$ fm) Wilson lattices. In a recent variational study on clover fermion [50], explicit $N\pi$ and $N\pi\pi$ interpolation fields are included in a variational calculation. Although $N(0)\pi(0)\pi(0)$ and $N(1)\pi(-1)$ states were found, the Roper mass still appears high. The authors conclude that the Roper is sensitive to the dynamics of the system, and good coupling to multi-hadron states such as $N\pi$ is essential to the creation of the Roper resonance. We postulate that with chiral fermion actions such as the overlap, such multi-hadron states are more readily created dynamically with only the nucleon interpolation field, and thus bring down the Roper mass; as opposed to with Wilson-type fermions, one has to explicitly include the multi-hadron interpolation fields.

6.3 Conclusion and Future Works

We have investigated the the Roper mass puzzle in lattice QCD, and discussed the mechanism with which the choice of operators and preservation of chiral symmetry can affect the mass of Roper. We found that with a careful choice of operators, the Roper mass can be brought down by $\sim 300\,MeV$, and can be further lowered by using a chiral fermion. A natural next step is to take all these factors into account in one calculation, by performing a variational study using overlap fermion and a suitable set of operators, and check if the result would be compatible with the SEB result with overlap fermion in Figure 6.1b.

Chapter 7

Summary and Outlook

We have utilized lattice QCD as a first principle framework to study hadronic properties. A number of numerical techniques are established to improve the signal. We have used overlap fermion on top of domain wall configurations to calculate the disconnected contribution to the momentum fraction carried by quarks in the nucleon for u, d, and s quark. We calculate both the 3-point and 2-point correlation function on three lattices with different pion masses, spacings, and volumes, and take ratio to extract the momentum fraction. The values are then renormalized, and extrapolated to physical pion mass, large volume, and continuum limit. Our result is found to be consistent with smaller error than the global analysis, and we suggest that it to be used to further constrain the global analysis. However, there is still work to be done on this topic. The $48^3 \times 96$ lattice we use in this study is at the physical pion mass, and with large volume. Improvement on the statistics of this lattice is much needed to further shrink the error. Furthermore, similar to $\langle x \rangle$, the second moment $\langle x^2 \rangle$ has no direct experimental measurements, and input from lattice QCD calculations is appreciated to constrain its value.

We have also investigated the Roper mass puzzle, and the discrepancy of the Roper mass among lattice calculations. Results from the Roper wave function study and the GSE method hint that care must be taken when choosing the size of the quark source. Calculation is then done with a clover lattice and the Roper mass is extracted with the variation method, which shows that with the appropriate smear sizes, result obtained this way is consistent with a previous calculation using a similar clover lattice, and the SEB fitting method. However, this result is still higher than the previous overlap result with the SEB method, which, when extrapolated to the physical pion mass, is consistent with the experimental value. We theorize that the difference is due to the distinct choice of fermion action, and that the Roper is sensitive to chiral symmetry. A further calculation with overlap fermion and the variation method is proposed to finally settle the discrepancy, and resolve the puzzle.

Bibliography

[1] J. Ashman et al., Physics Letters B **2**06, 364 (1988).

[2] P. H. Ginsparg and K. G. Wilson, Physical Review D **2**5, 2649 (1982).

[3] H. Neuberger, Physics Letters B 427, 353 (1998), arXiv:hep-lat/9801031.

[4] J. v. d. Eshof, A. Frommer, T. Lippert, K. Schilling, and H. A. van der Vorst, Computer Physics Communications **1**46, 203 (2002), arXiv: hep-lat/0202025.

[5] S. Güsken, Nuclear Physics B - Proceedings Supplements **1**7, 361 (1990).

[6] C. Alexandrou, S. Güsken, F. Jegerlehner, K. Schilling, and R. Sommer, Nucl. Phys. B **4**14, 815 (1994).

[7] S.-J. Dong and K.-F. Liu, Phys. Lett. C **3**28, 130 (1994), arXiv:hep-lat/9308015.

[8] A. Li et al., Phys. Rev. D **8**2, 114501 (2010), arXiv:1005.5424.

[9] T.-W. Chiu and S. V. Zenkin, Phys. Rev. D **5**9 (1999), arXiv:hep-lat/9806019.

[10] K. F. Liu and S. J. Dong, Int. J. Mod Phys A **2**0, 7241 (2005), arXiv:hep-lat/0206002.

[11] W. Wilcox, PoS **L**ATTICE2007 (2007), arXiv: 0710.1813.

[12] M Lüscher, Nuclear Physics B **3**39, 222 (1990).

[13] M. Deka et al., Phys. Rev. D **7**9, 094502 (2009).

[14] T. Doi et al., PoS **L**ATTICE2008 (2008), arXiv: 0810.2482.

[15] X. Ji, Phys. Rev. Lett. **7**8, 610 (1997).

[16] Y. Aoki et al., arXiv:1011.0892 (2010), Phys.Rev.D83:074508,2011.

[17] RBC et al., arXiv:1411.7017 [hep-lat] (2014), arXiv: 1411.7017.

[18] L. Maiani, G. Martinelli, M. L. Paciello, and B. Taglienti, Nuclear Physics B **2**93, 420 (1987).

[19] D. B. Renner, arXiv:1002.0925 [hep-lat] (2010), arXiv: 1002.0925.

[20] P. M. Nadolsky et al., Physical Review D **7**8 (2008).

[21] P. C. Bruns, L. Greil, R. Rödl, and A. Schäfer, arXiv:1411.7528 [hep-lat, physics:hep-ph] (2014), arXiv: 1411.7528.

[22] M. Lujan et al., Physical Review D **8**6 (2012), arXiv:1204.6256.

[23] A. D. Martin, W. J. Stirling, R. S. Thorne, and G. Watt, The European Physical Journal C **6**3, 189 (2009), arXiv: 0901.0002.

[24] K.-F. Liu, W.-C. Chang, H.-Y. Cheng, and J.-C. Peng, Phys. Rev. Lett. **1**09, 252002 (2012).

[25] J. C. Peng, W. C. Chang, H. Y. Cheng, and K. F. Liu, arXiv:1402.1236 (2014), arXiv: 1402.1236.

[26] K. Ackerstaff et al., Physical Review Letters **8**1, 5519 (1998).

[27] H.-L. Lai et al., Physical Review D **8**2 (2010).

[28] T. Barnes and F. Close, Physics Letters B **1**23, 89 (1983).

[29] S. Capstick, Progress in Particle and Nuclear Physics **4**5, S241 (2000), arXiv:nucl-th/0008028.

[30] K. F. Liu and C. W. Wong, Physical Review D **2**8, 170 (1983).

[31] S. Capstick and N. Isgur, Physical Review D **3**4, 2809 (1986).

[32] K. F. Liu, J. S. Zhang, and G. R. E. Black, Physical Review D **3**0, 2015 (1984).

[33] J. D. Breit and C. R. Nappi, Physical Review Letters **5**3, 889 (1984).

[34] U. B. Kaulfuss and U.-G. Meissner, Physics Letters B **1**54, 193 (1985).

[35] R. Jaffe and F. Wilczek, The European Physical Journal C **3**3, s38 (2004), arXiv:hep-ph/0401034.

[36] N. Mathur et al., Physics Letters B **6**05, 137 (2005), arXiv: hep-ph/0306199.

[37] B. G. Lasscock et al., Physical Review D **7**6 (2007).

[38] M. S. Mahbub, W. Kamleh, D. B. Leinweber, P. J. Moran, and A. G. Williams, Physics Letters B **7**07, 389 (2012), arXiv: 1011.5724.

[39] R. G. Edwards, J. J. Dudek, D. G. Richards, and S. J. Wallace, Phys. Rev. D **8**4, 074508 (2011).

[40] G. P. Engel, C. B. Lang, D. Mohler, and A. Schäfer, PoS **H**adron2013 (2013), arXiv:1311.6579.

[41] C. Alexandrou, T. Korzec, G. Koutsou, and T. Leontiou, Physical Review D **8**9 (2014), arXiv: 1302.4410.

[42] Ying Chen et al., (2004), arXiv:hep-lat/0405001.

[43] Y. Chen, Modern Physics Letters A **2**2, 583 (2007).

[44] D. S. Roberts, W. Kamleh, and D. B. Leinweber, Physics Letters B **7**25, 164 (2013), arXiv: 1304.0325.

[45] A. Matsuyama, T. Sato, and T.-S. Lee, Physics Reports **4**39, 193 (2007).

[46] N. Suzuki et al., Phys. Rev. Lett. **1**04, 042302 (2010), arXiv:0909.1356.

[47] L. Glozman and D. Riska, Physics Reports **2**68, 263 (1996).

[48] W. Bardeen, A. Duncan, E. Eichten, N. Isgur, and H. Thacker, Physical Review D **6**5 (2001).

[49] N. Mathur et al., Physical Review D **7**6 (2007).

[50] C. B. Lang, L. Leskovec, M. Padmanath, and S. Prelovsek, arXiv:1610.01422 [hep-lat, physics:hep-ph, physics:nucl-ex, physics:nucl-th] (2016), arXiv: 1610.01422.

Vita

Education

- Doctor of Philosophy: Department of Physics and Astronomy, University of Kentucky, 2016 (expected).
  - Thesis: Lattice QCD calculation of momentum fraction carried by quarks in the nucleon, and the roper puzzle
  - Director: Professor Keh-Fei Liu
- Master of Science (Physics): Department of Physics and Astronomy, University of Kentucky.
- Bachelor of Science (Physics): Department of Physics, Nanjing University, China.

Professional experience

- Augest 2009–Augest 2016: Teaching assistant & research assistant, Department of Physics and Astronomy, University of Kentucky.